

Heavy-quark mass dependence in global PDF analyses and 3- and 4-flavour parton distributions

A.D. MARTIN^a, W.J. STIRLING^b, R.S. THORNE^c AND G. WATT^d

^a Institute for Particle Physics Phenomenology, University of Durham, DH1 3LE, UK

^b Cavendish Laboratory, University of Cambridge, CB3 0HE, UK

^c Department of Physics and Astronomy, University College London, WC1E 6BT, UK

^d Theory Group, Physics Department, CERN, CH-1211 Geneva 23, Switzerland

Abstract

We study the sensitivity of our recent MSTW 2008 NLO and NNLO PDF analyses to the values of the charm- and bottom-quark masses, and we provide additional public PDF sets for a wide range of these heavy-quark masses. We quantify the impact of varying m_c and m_b on the cross sections for W , Z and Higgs production at the Tevatron and the LHC. We generate 3- and 4-flavour versions of the (5-flavour) MSTW 2008 PDFs by evolving the input PDFs and α_S determined from fits in the 5-flavour scheme, including the eigenvector PDF sets necessary for calculation of PDF uncertainties. As an example of their use, we study the difference in the Z total cross sections at the Tevatron and LHC in the 4- and 5-flavour schemes. Significant differences are found, illustrating the need to resum large logarithms in Q^2/m_b^2 by using the 5-flavour scheme. The 4-flavour scheme is still necessary, however, if cuts are imposed on associated (massive) b -quarks, as is the case for the experimental measurement of $Zb\bar{b}$ production and similar processes.

1 Introduction

Parton distribution functions (PDFs) determined from global analysis [1–5] of fixed-target and collider data, mainly from deep-inelastic scattering (DIS), are an essential input to theory calculations for hard processes at hadron colliders such as the Tevatron and LHC. In addition to the fitted input PDFs, several other parameters enter into the global fits, which affect both the PDFs obtained and predictions for hadronic processes. One important example is the value of the strong coupling α_S and its uncertainty [6–8]. Others, which are the focus of the present paper, are the values of the heavy-quark masses and the scheme used to calculate heavy-quark contributions to observables. In particular, while the precise values taken for m_c and m_b may not be crucial for the processes included in the global PDF analyses, calculations of processes with explicit c - and b -quarks might be more sensitive to these values, and it is therefore desirable to have PDFs available which have been consistently fitted and evolved with corresponding values of m_c and m_b .

We will study two topics, both of which concern the treatment of the heavy charm and bottom quarks in global parton analyses. The first topic, which is the subject of Section 3, concerns the sensitivity of the MSTW 2008 global parton analysis [1] to the values of the heavy-quark masses m_h , with $h = c, b$. In Ref. [1] these masses were taken to be $m_c = 1.40$ GeV and $m_b = 4.75$ GeV. Here we perform global fits for a range of m_c and m_b about these values, with $\alpha_S(M_Z^2)$ allowed to be a free parameter. In this way, we determine the values of m_c and m_b preferred by the data, and the correlations between these values of m_h and $\alpha_S(M_Z^2)$. Due to a significant correlation between m_c and $\alpha_S(M_Z^2)$, we also perform fits with varying m_c but with $\alpha_S(M_Z^2)$ held fixed. We study how the cross sections for W , Z and Higgs boson production at the Tevatron and the LHC depend on the choice of m_c and m_b , and we provide a recommendation on how to include the uncertainty arising from m_h in a general cross-section calculation.

The second topic, described in Section 4, is the generation of sets of 3- and 4-flavour PDFs corresponding to the MSTW 2008 [1] 5-flavour sets of PDFs. We follow the same procedure previously used to generate the 3- and 4-flavour versions [9] of the 5-flavour MRST 2004 PDFs [10], i.e. the input PDFs (and α_S) at $Q_0^2 = 1$ GeV² determined from fits in the 5-flavour scheme are used as the initial condition for 3- or 4-flavour evolution. However, going beyond Ref. [9], we also provide 3- and 4-flavour *eigenvector* PDF sets to enable calculation of PDF uncertainties, and we provide 3- and 4-flavour PDF sets for a wide range of m_c and m_b values, respectively. As an example of the use of the central 4-flavour PDFs for the default quark masses, we compare the total cross sections for Z production at the Tevatron and LHC in the 4- and 5-flavour schemes. However, first we begin with a short résumé of the alternative “schemes” to treat heavy flavours¹, and in particular, an explanation of what precisely we mean by 3-, 4-, and 5-flavour PDFs.

¹Strictly speaking, it would be better to say alternative “techniques”, since the use of the word “scheme” is usually reserved for an alternative choice in the ordering of the perturbative expansion, or a particular separation of contributions between the coefficient functions and parton densities—an ambiguity inherent in QCD.

2 Schemes for the treatment of heavy flavours

It is appropriate to briefly recall the various schemes for the treatment of heavy flavours in global parton analyses. In PDF analyses it is common to start evolving upwards from $Q^2 = Q_0^2 \sim 1 \text{ GeV}^2$ with the distributions of the three light quarks (u, d, s), assuming that they are massless. As we evolve upwards, we have the choice to turn on the heavy-quark (c, b, t) distributions as we pass through their respective transition point, for which a convenient choice is $\mu_F^2 = m_h^2$. As we pass through a transition point, the number of active quarks is increased from n to $n + 1$, and the parton densities are related to each other perturbatively, i.e.

$$f_j^{n+1}(\mu_F^2) = \sum_k A_{jk}(\mu_F^2/m_h^2) \otimes f_k^n(\mu_F^2), \quad (1)$$

where the perturbative matrix elements $A_{jk}(\mu_F^2/m_h^2)$ contain $\ln(\mu_F^2/m_h^2)$ terms which are known to $\mathcal{O}(\alpha_S^2)$ [11] and $\mathcal{O}(\alpha_S^3)$ [12]. The “ x ” arguments have been suppressed in Eq. (1), and the symbol \otimes is shorthand for the convolution

$$f \otimes g \equiv \int_x^1 \frac{dx'}{x'} f(x')g(x/x'). \quad (2)$$

Eq. (1) relates the $f_i^n(\mu_F^2)$ set of partons to the $f_i^{n+1}(\mu_F^2)$ set, guaranteeing the correct evolution for both the n and $n + 1$ regimes. We make the simplest choice, $\mu_F^2 = Q^2$, for the factorisation scale.

Hence, we have to decide whether or not to keep a heavy quark as just a final-state particle, and not as a parton within the proton. We may choose to keep just the three light flavours as parton distributions. We will call this the 3-flavour scheme (3FS), though it is often referred to as the fixed flavour number scheme (FFNS). Alternatively, we may include the c -quark in the evolution above $Q^2 = m_c^2$ and generate 4-flavour PDFs in a 4-flavour scheme (4FS). Actually, in the global MRST/MSTW parton analyses we also include the b -quark distribution in the evolution above $Q^2 = m_b^2$, but *not* the t -quark above $Q^2 = m_t^2$, so we generate 5-flavour sets of parton distributions in a 5-flavour scheme (5FS). So to be precise, in our definition of n_f -flavour parton sets, n_f refers to the *maximum* number of quark flavours in the evolution.

In each n_f -flavour scheme (n_f FS) the structure functions are given by the usual convolution of coefficient functions and parton distributions:

$$F(x, Q^2) = \sum_j C_j^{n_f\text{FS}}(Q^2/m_h^2) \otimes f_j^n(Q^2), \quad (3)$$

where the sum j is over the gluon and the (variable, depending on Q^2) number of active quark flavours, $n \leq n_f$. We have a choice in how to choose n_f and define the coefficient functions. One simple choice is to fix $n = n_f = 3$. For the heavy flavours, all the m_h dependence then occurs in the coefficient functions, and these are called the FFNS coefficient functions. The structure functions may be written in the form

$$F(x, Q^2) = \sum_{j=u,d,s,g} C_j^{\text{FF},3}(Q^2/m_h^2) \otimes f_j^3(Q^2). \quad (4)$$

However, the sum of the $\alpha_S^k \ln^m(Q^2/m_h^2)$ terms, with $m \leq k$, is not included in the perturbative expansion. Thus the accuracy of the expansion becomes increasingly unreliable as Q^2 increases above m_h^2 . In addition, there is the problem that the full mass dependence of the coefficient functions is known up to NLO [13], but is not completely defined at NNLO, i.e. the α_S^3 coefficient, $C_{2,hg}^{\text{FF},3,(3)}$, for F_2 is not fully known, see Ref. [12]. (Here, the outer subscript “ hg ” denotes the $g \rightarrow h$ contribution to the heavy-flavour structure function F_2^h .)

As an aside, we note that it would be possible to treat the charm quark as light, and the bottom quark as heavy. Then it would be possible to express the structure functions and cross sections in terms of four light quarks with all the mass dependence of the bottom quark contained in the coefficient functions. This is sometimes called the 4-flavour FFNS. However if one needs to use scales $Q^2 < m_b^2$ and in the vicinity of m_c^2 , as for example in the global PDF analysis, then the charm-quark mass dependence, and the charm transition point (if $Q^2 \leq m_c^2$), should be included. Thus, this 4-flavour FFNS is only applicable in a restricted range of Q^2 , and it will not be considered further here.

The alternative, and better, approach is to use the 4-flavour (and 5-flavour) PDFs of the variable flavour number schemes (4FS, 5FS). The simplest variable flavour number evolution procedure is to evolve treating some (or all) of the heavy quarks as massless, but to turn on the distributions at the appropriate transition points, $Q^2 = m_h^2$. That is, to assume that these heavy-quark distributions evolve according to the splitting functions for massless quarks. Thus, the resummation of the large logarithms in Q^2/m_h^2 is achieved by the introduction of heavy-flavour parton distributions and the solution of the evolution equations. It is motivated by the observation that at high scales the massive quarks behave like massless partons, and the coefficient functions are simply those in the massless limit, e.g. for structure functions

$$F(x, Q^2) = \sum_j C_j^{n_f \text{ZMVF}} \otimes f_j^n(Q^2), \quad (5)$$

where, as in Eq. (3), the sum j is over the gluon and the (variable) number $n \leq n_f$ of quarks that are active during the evolution. This is the so-called zero-mass variable flavour number scheme (ZM-VFNS). However, the ZM-VFNS has the failing that it simply ignores $\mathcal{O}(m_h^2/Q^2)$ corrections to the coefficient functions, and hence it is inaccurate in the region where Q^2 is not so much greater than m_h^2 . Thus, strictly speaking, the ZM-VFNS does not define a scheme, but rather an approximation.

So we have two approaches where the treatment of heavy flavours is relatively simple. The 3-flavour scheme (or FFNS), appropriate to the region $Q^2 \lesssim m_c^2$, and the ZM-VFNS, appropriate to the region $Q^2 \gg m_h^2$. Clearly, for precision parton analyses, we must use a so-called general-mass variable flavour number scheme (GM-VFNS) which smoothly connects these two well-defined regions, so as to reduce to the (3-flavour) FFNS in the low Q^2 limit and to the ZM-VFNS in the high Q^2 limit (up to possible terms of higher order in α_S). In particular, in Eq. (3) the value of n increases by one each time we reach $Q^2 = m_h^2$ in the evolution, and the coefficient functions $C_j^{n_f \text{GMVF}}(Q^2/m_h^2)$ interpolate smoothly from $C_j^{\text{FF},3}(Q^2/m_h^2)$ to $C_j^{n_f \text{ZMVF}}$,

for the maximum value of $n = n_f$. There is some freedom in how one does this, and in the MSTW 2008 analysis [1] we use the definition of the GM-VFNS as described in Ref. [14].² We also note that actually a 5-flavour GM-VFNS is used, since we do not include the top quark in the evolution. Note that this means that processes such as associated production of Higgs bosons with top quarks should be calculated using the 5-flavour PDFs with the full $2 \rightarrow 3$ subprocess matrix elements, i.e. $gg, q\bar{q} \rightarrow Ht\bar{t}$. In a 6FS, one would calculate this via $t\bar{t} \rightarrow H$, introducing a top-quark PDF. Although in principle this method would include resummed higher-order corrections $\sim [\alpha_S \ln(M_H^2/m_t^2)]^n$, we would expect that for all practical purposes³ at the LHC, the 5FS approach, $gg, q\bar{q} \rightarrow Ht\bar{t}$, supplemented by NLO corrections, would be adequate, see also Section 4.2.

As just noted, the use of a GM-VFNS is nowadays essential for the determination of a set of precision PDFs from the data.⁴ However, there are processes where the full mass dependence of the coefficient functions for c and b production processes are only known in the case where the heavy quark is treated as a final-state particle, and not as a parton in the proton. For example, FFNS parton distributions are needed for use with the HVQDIS [19, 20] and MC@NLO [21] programs. Thus in this paper we make available 3- and 4-flavour PDFs. We also give an example of their use. This is the subject of Section 4.

3 Dependence of PDFs on the heavy-quark masses

In the MSTW 2008 global parton analysis [1] we used $m_c = 1.40$ GeV and $m_b = 4.75$ GeV, where these are the pole mass values. Some limited justification for choosing these values was briefly given at the end of Section 3 of Ref. [1]. To summarise, there was little data constraint on m_b , so it was simply fixed at a value of 4.75 GeV, close to the calculated $\overline{\text{MS}}$ mass transformed to the pole mass. The fixed value of $m_c = 1.40$ GeV was close to the best-fit value at NLO if treated as a free parameter, but a little higher than the best-fit value at NNLO, and lower than the calculated $\overline{\text{MS}}$ mass transformed to the pole mass. We discuss limitations in constraints on the pole masses by transforming from the calculated $\overline{\text{MS}}$ masses below in Section 3.3.

Here, using *exactly* the same data sets, we repeat the global analysis for different fixed values of m_c and m_b , but with $\alpha_S(M_Z^2)$ left as a free parameter. The MSTW 2008 global fit [1] used a wide variety of data from both fixed-target experiments and the HERA ep and Tevatron $p\bar{p}$ colliders. Neutral-current structure functions (F_2 and F_L) were included from fixed-target lepton–nucleon scattering experiments (BCDMS [22, 23], NMC [24, 25], E665 [26] and

²At NNLO this involves some modelling of the $\mathcal{O}(\alpha_S^3)$ FFNS coefficient functions which are not fully calculated. In the GM-VFNS we only need these in the low- Q^2 regime and we approximate them using the known results of the small- x [15] and threshold limits [16] (see Refs. [17, 18] for recent refinements).

³Note that for $M_H \lesssim 1$ TeV, $\alpha_S \ln(M_H^2/m_t^2) \lesssim 0.35$.

⁴In fact we only use the GM-VFNS for structure functions in DIS, whereas hadron collider cross sections are calculated in the ZM-VFNS under the assumption that mass effects are negligible at the typically large scales. (Low-mass fixed-target Drell–Yan production is also calculated in the ZM-VFNS, but here heavy flavours contribute $\ll 1\%$ of the total, so inaccuracies induced by using the ZM-VFNS are in practice irrelevant.)

(a) NLO:

m_c (GeV)	χ_{global}^2 (2699 pts.)	$\chi_{F_2^c}^2$ (83 pts.)	$\alpha_S(M_Z^2)$
1.1	2729	263	0.1182
1.2	2625	188	0.1188
1.3	2563	134	0.1195
1.4	2543	107	0.1202
1.45	2541	100	0.1205
1.5	2545	97	0.1209
1.6	2574	104	0.1216
1.7	2627	128	0.1223

(b) NNLO:

m_c (GeV)	χ_{global}^2 (2615 pts.)	$\chi_{F_2^c}^2$ (83 pts.)	$\alpha_S(M_Z^2)$
1.1	2498	113	0.1159
1.2	2463	88	0.1162
1.26	2456	82	0.1165
1.3	2458	82	0.1166
1.4	2480	95	0.1171
1.5	2528	126	0.1175
1.6	2589	167	0.1180
1.7	2666	217	0.1184

Table 1: Fit quality and $\alpha_S(M_Z^2)$ for different m_c values at (a) NLO and (b) NNLO.

SLAC [27–29]), low-mass Drell–Yan cross sections from the E866/NuSea experiment [30, 31], and charged-current structure functions (F_2 and xF_3) and dimuon cross sections from neutrino–nucleon scattering experiments (CCFR/NuTeV [32, 33] and CHORUS [34]). From the HERA experiments, H1 and ZEUS, data were included on neutral- and charged-current reduced cross sections (σ_r^{NC} and σ_r^{CC}) [35–43], the charm structure function (F_2^c) [44–50], and inclusive jet production in DIS [51–53]. From the Tevatron experiments, CDF and DØ, Run II data were included on inclusive jet production [54, 55], the lepton charge asymmetry from W decays [56, 57] and the Z rapidity distribution [58, 59]. A more detailed description of the treatment of each of these data sets can be found in Ref. [1]. Note that more precise H1 and ZEUS data on F_2^c (and the beauty structure function, F_2^b , not included originally) are now available, but we stick to fitting exactly the same data sets as in the MSTW 2008 analysis.

3.1 Dependence on charm-quark mass m_c

The sensitivity to the charm mass of the data in the global PDF analysis, and the subset of F_2^c data, in terms of the goodness-of-fit measure χ^2 , is shown in Table 1 at NLO and NNLO. The global best-fit values of m_c , found by varying m_c in steps of 0.01 GeV, are $m_c = 1.45$ GeV at NLO and $m_c = 1.26$ GeV at NNLO. Recall that in Section 3 of Ref. [1] we instead quoted best-fit values of $m_c = 1.39$ GeV at NLO and $m_c = 1.27$ GeV at NNLO. In fact, the more detailed analysis performed here, by scanning m_c in steps of 0.01 GeV, revealed a rather flat minimum of the global χ^2 versus m_c , with a slight double-minimum structure at NLO (the two minima being at 1.39 GeV and 1.45 GeV). Hence the best-fit values we quote here, of $m_c = 1.45$ GeV at NLO and $m_c = 1.26$ GeV at NNLO, differ slightly from the best-fit values given in Ref. [1]. Note from Table 1(a) that there is a clear correlation between m_c and the value of $\alpha_S(M_Z^2)$ obtained from the NLO fit, and that from Table 1(b) this correlation is reduced at NNLO.

In Fig. 1 we show the NLO and NNLO global χ^2 profiles as a function of m_c . We see that at NLO there is a preference for $m_c = 1.45$ GeV, with a 1σ uncertainty of ${}^{+0.14}_{-0.06}$ GeV. The global

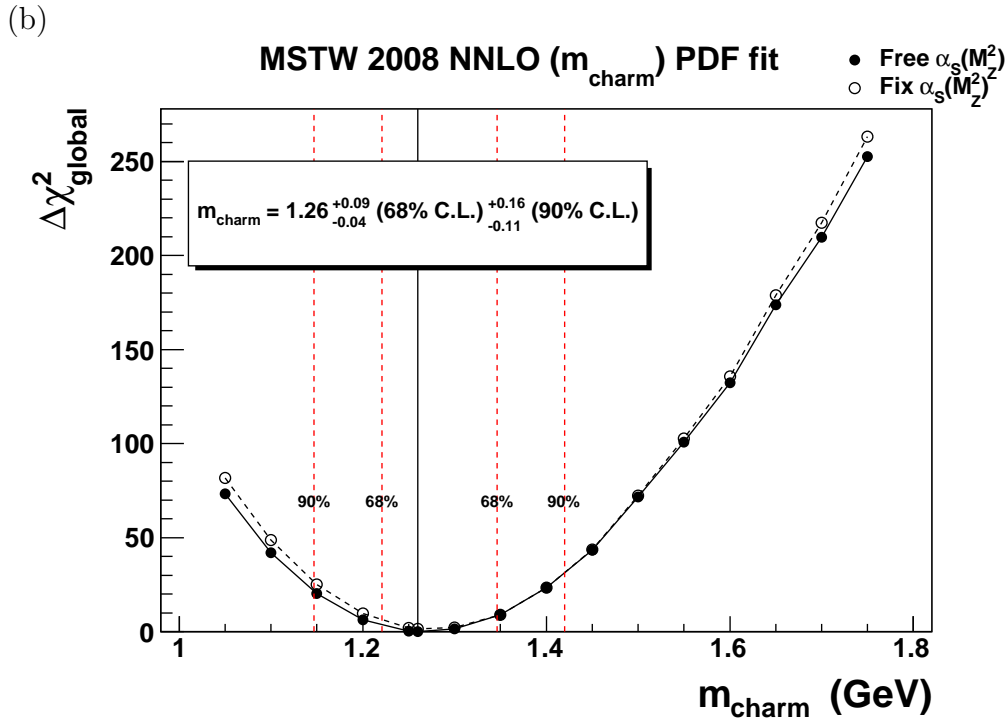
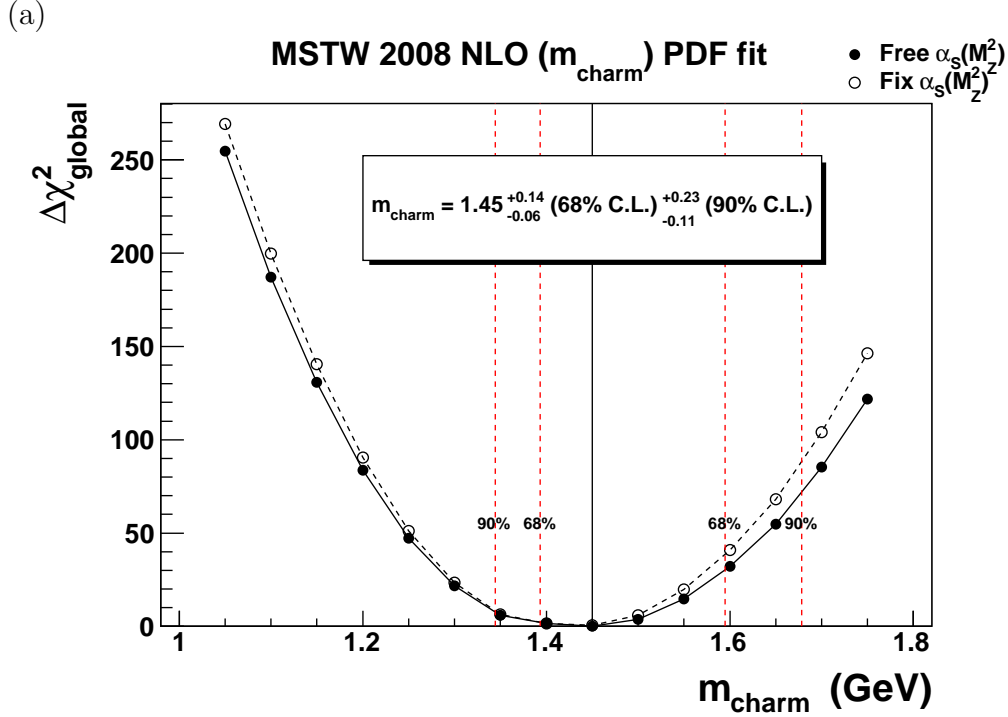


Figure 1: Dependence on m_c of the global χ^2 , relative to the value at the best-fit m_c , at (a) NLO and (b) NNLO, fitting to the same data sets used in the MSTW 2008 global analysis [1]. The values quoted for m_c correspond to treating $\alpha_s(M_Z^2)$ as a free parameter, and the corresponding global χ^2 values are shown by the *closed points* (●) joined by the *continuous curves*. The 68% (1σ) and 90% confidence-level (C.L.) uncertainties on m_c are indicated by the *vertical dashed lines*. The *open points* (○), joined by the *dashed curves*, are the global χ^2 values with $\alpha_s(M_Z^2)$ held fixed.

data prefer a lower value of m_c at NNLO, namely $m_c = 1.26$ GeV, with a 1σ uncertainty of $^{+0.09}_{-0.04}$ GeV. (For the higher values of m_c , the NNLO fit considerably undershoots the moderate Q^2 deep-inelastic data.) Here, the 1σ uncertainty is obtained in exactly the same way as described for the uncertainty on $\alpha_S(M_Z^2)$ in Ref. [6], i.e. by examining the χ^2 profile of each data set included in the global fit. The distinguishing power of the various data sets is shown in Fig. 2. Here, the points (\bullet) indicate the values of m_c for which the χ^2 for each data set is minimised (within the context of the global fit), while the inner error bars extend across the 68% confidence-level (C.L.) region and the outer error bars extend across the 90% C.L. region (see Section 4 of Ref. [6] for the precise definitions of the 68% and 90% C.L. limits). As may be expected, the $F_2^c(x, Q^2)$ data of the H1 and ZEUS collaborations are the most discriminating. Indeed, they dominate the determination of m_c , as can be seen from Fig. 3, which shows χ^2 versus m_c for the F_2^c data alone. For the HERA inclusive data, changes in the value of m_c are partially compensated by changes in the gluon and in α_S . The NMC data prefer a lower value of m_c giving a quicker evolution near threshold. Similarly the BCDMS data mainly prefer a lower m_c , but only due to the correlation with a lower value of α_S . Supplementary plots of the χ^2 profiles versus m_c for all data sets in the global fit are available from Ref. [60]. The experimental uncertainty on m_c , given in Fig. 1 and indicated by the horizontal dashed lines in Fig. 2, is chosen to ensure that all data sets are described within their 68% or 90% C.L. limits.

The dependence of the PDFs on the value taken for m_c is shown in Fig. 4. The plots show the ratio of the NLO PDFs obtained with $m_c = 1.3$ GeV and $m_c = 1.5$ GeV to those of the MSTW 2008 analysis (which assumed $m_c = 1.4$ GeV) at scales of $Q^2 = 4$ GeV² and $Q^2 = 10^4$ GeV². We see that the ratios lie well within the 90% C.L. PDF uncertainty. The exception is the charm distribution at $Q^2 = 4$ GeV² where, as expected, the different charm transition points have an appreciable effect.

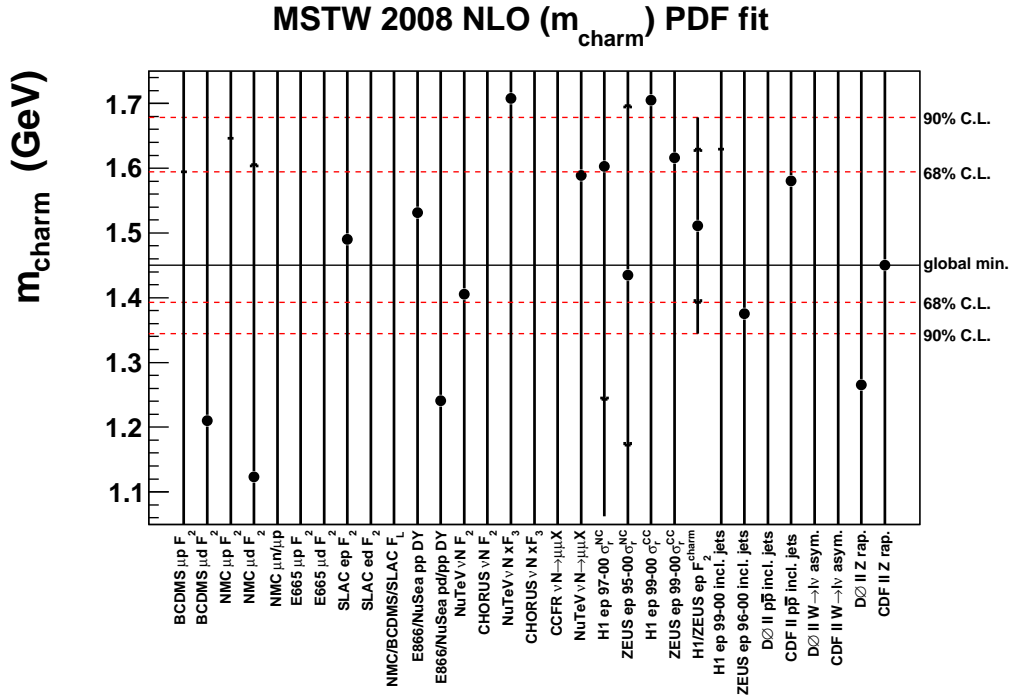
3.2 Dependence on bottom-quark mass m_b

We repeated the whole exercise for m_b . That is, we performed a series of global fits for different values of m_b . The results are shown in Table 2. Now there is less sensitivity to the value of the quark mass, and essentially no correlation between m_b and $\alpha_S(M_Z^2)$. Indeed, the global χ^2 stays fairly flat all the way down to $m_b = 3$ GeV. For the lower values of m_b , there is a slightly better description of the HERA data, including $F_2^c(x, Q^2)$. A similar conclusion holds at NNLO, but with about half the change in global χ^2 , that is, even less sensitivity to m_b .

Note that the HERA $F_2^b(x, Q^2)$ data [46,47,61–63] are not included in the global fits, neither in MSTW 2008 [1], nor in the fits described above. In Fig. 5 we compare the predictions of the NNLO fits with varying m_b values to the F_2^b data from H1 [61]. We also show a few of the (less precise) ZEUS data points [62]. In Table 2 we give the χ^2 for the H1 F_2^b data accounting⁵ for all 24 sources of correlated systematic uncertainty, and we also give the simple addition with

⁵We use Eqs. (38–40) of Ref. [1], noting that there is a typo in Eq. (40) of that paper and $\sigma_{n,i}^{\text{uncorr.}}$ should appear squared in the expression for $A_{kk'}$.

(a)



(b)

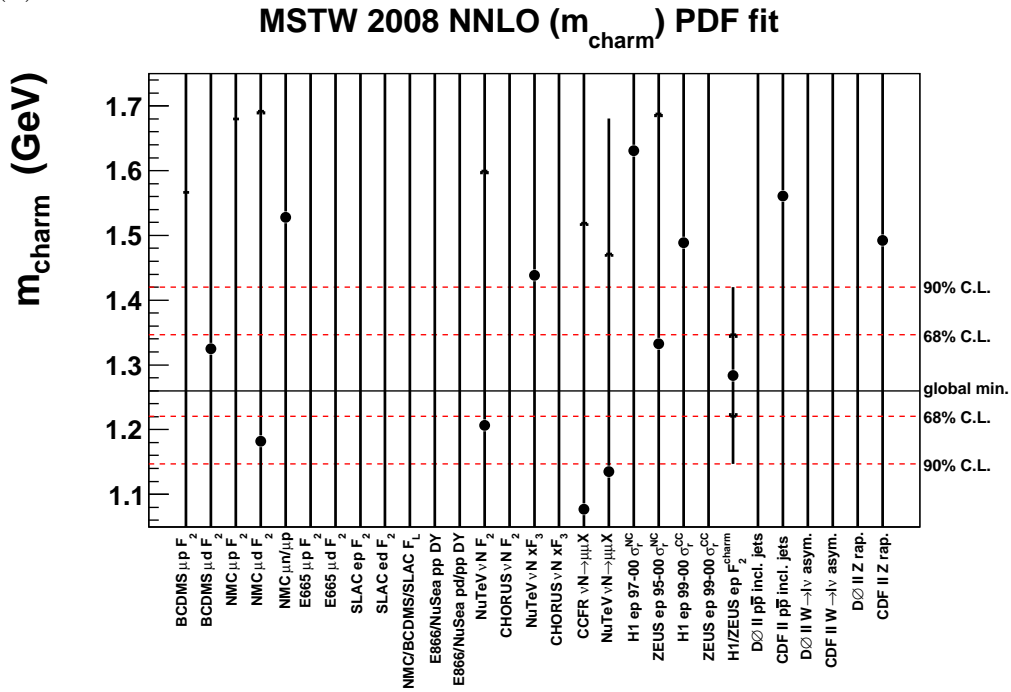
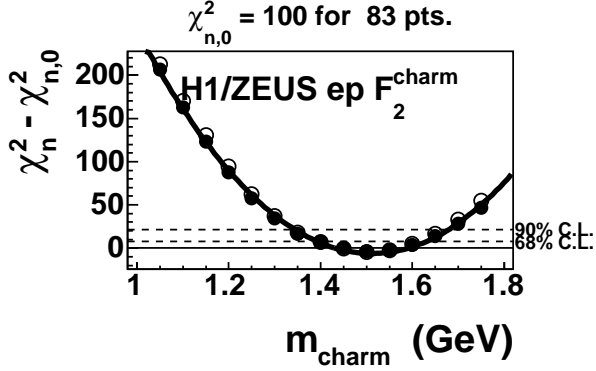


Figure 2: Ranges of m_c for which data sets are described within their 90% C.L. limit (*outer error bars*) or 68% C.L. limit (*inner error bars*) in the (a) NLO and (b) NNLO global fits, with $\alpha_S(M_Z^2)$ as a free parameter. The *points* (\bullet) indicate the values of m_c favoured by each individual data set, that is, the values for which the χ^2 is minimised. The experimental uncertainty on m_c , indicated by the *horizontal dashed lines*, is chosen to ensure that all data sets are described within their 68% or 90% C.L. limits defined by Eq. (2) of Ref. [6].

(a) MSTW 2008 NLO:



(b) MSTW 2008 NNLO:

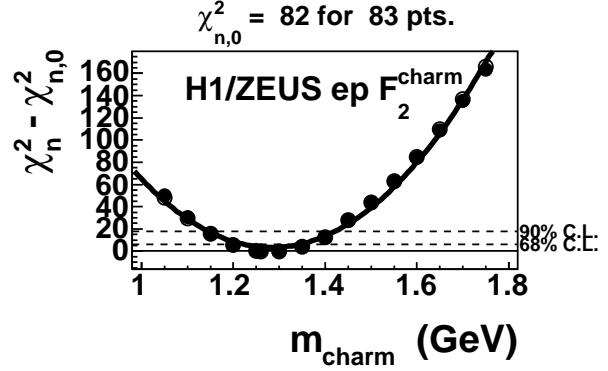


Figure 3: Dependence on m_c of the χ^2 for HERA data [44–50] on the charm structure function, F_2^c , relative to the value at the global best-fit m_c , at (a) NLO and (b) NNLO. The *closed points* (\bullet) have $\alpha_S(M_Z^2)$ as a free parameter, and are fitted to a quadratic function of m_c shown by the continuous curves, while the *open points* (\circ , mostly hidden) have $\alpha_S(M_Z^2)$ held fixed at the MSTW 2008 value. The *horizontal dashed lines* in the plots indicate the 68% and 90% C.L. limits, determined according to a “hypothesis-testing” criterion, see Section 4 of Ref. [6].

m_b (GeV)	NLO				NNLO			
	χ_{global}^2 (2699 pts.)	$\chi_{F_2^b}^2$ (12 pts.)	$\chi_{\text{global}+F_2^b}^2$ (2711 pts.)	$\alpha_S(M_Z^2)$	χ_{global}^2 (2615 pts.)	$\chi_{F_2^b}^2$ (12 pts.)	$\chi_{\text{global}+F_2^b}^2$ (2627 pts.)	$\alpha_S(M_Z^2)$
4.00	2537	20	2557	0.1202	2477	21	2498	0.1171
4.25	2539	13	2552	0.1202	2478	15	2493	0.1171
4.50	2541	8.9	2550	0.1202	2478	11	2489	0.1171
4.75	2543	7.4	2550	0.1202	2480	8.8	2489	0.1171
5.00	2545	7.6	2553	0.1202	2481	6.9	2488	0.1170
5.25	2547	7.6	2555	0.1201	2483	7.7	2491	0.1170
5.50	2549	8.0	2557	0.1201	2485	7.9	2493	0.1170

Table 2: Fit quality and $\alpha_S(M_Z^2)$ for different m_b values at NLO and NNLO. Note that the F_2^b data [61] are not included in the global fit.

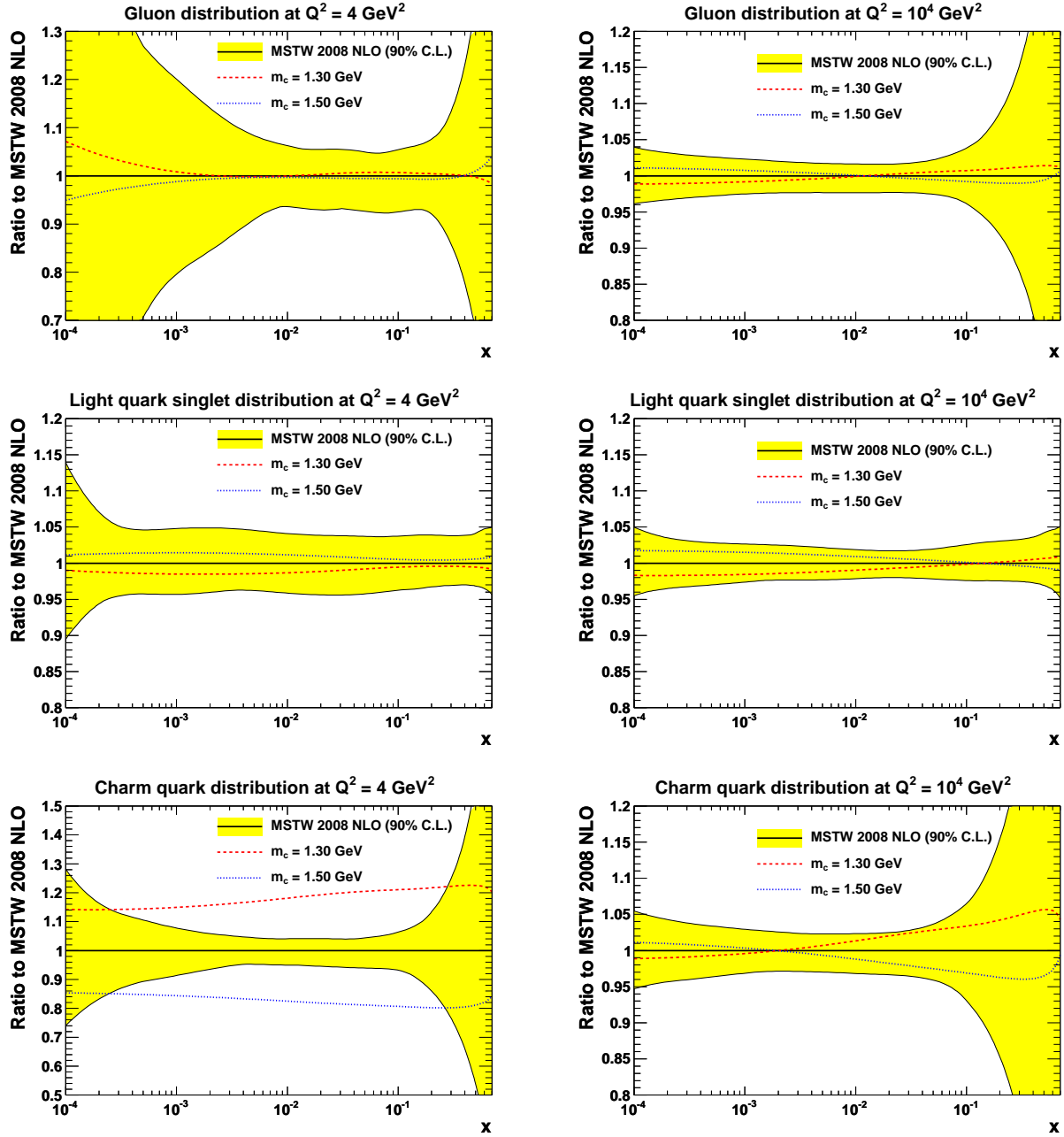


Figure 4: m_c dependence of gluon, singlet and charm distributions at NLO at two different Q^2 values, 4 GeV^2 (left) and 10^4 GeV^2 (right), compared to the 90% C.L. PDF uncertainties.

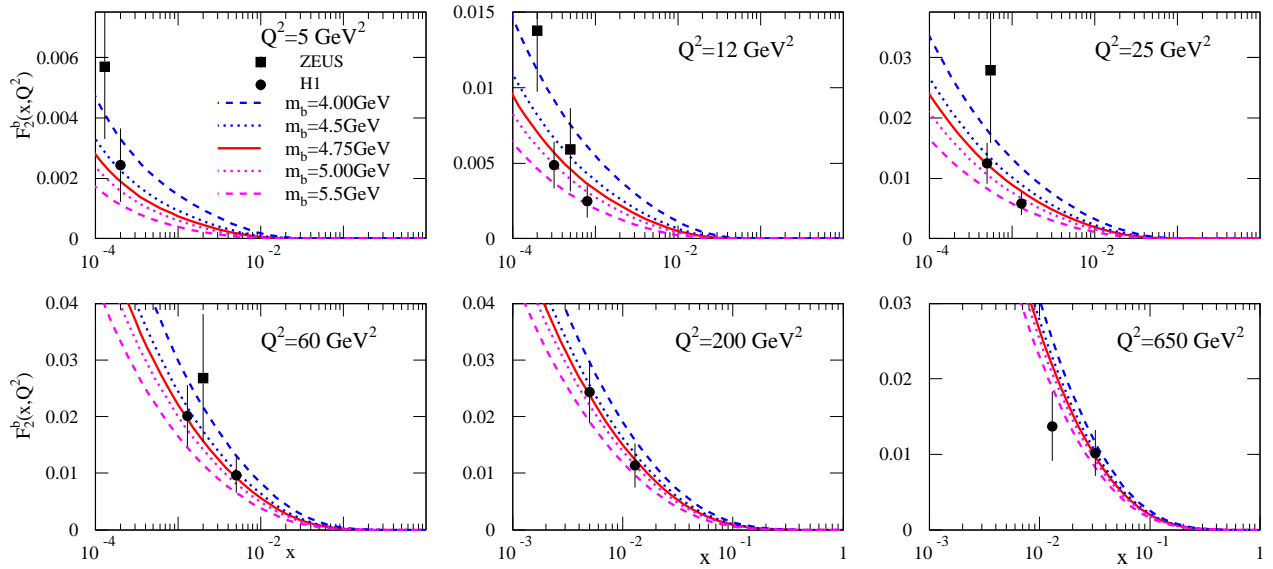


Figure 5: Comparison of the HERA $F_2^b(x, Q^2)$ data [61, 62] with NNLO predictions obtained using PDFs from global fits with different values of m_b . Note that the F_2^b data are not included in these global fits. The *curves*, in decreasing order, correspond to $m_b = 4, 4.5, 4.75, 5, 5.5 \text{ GeV}$.

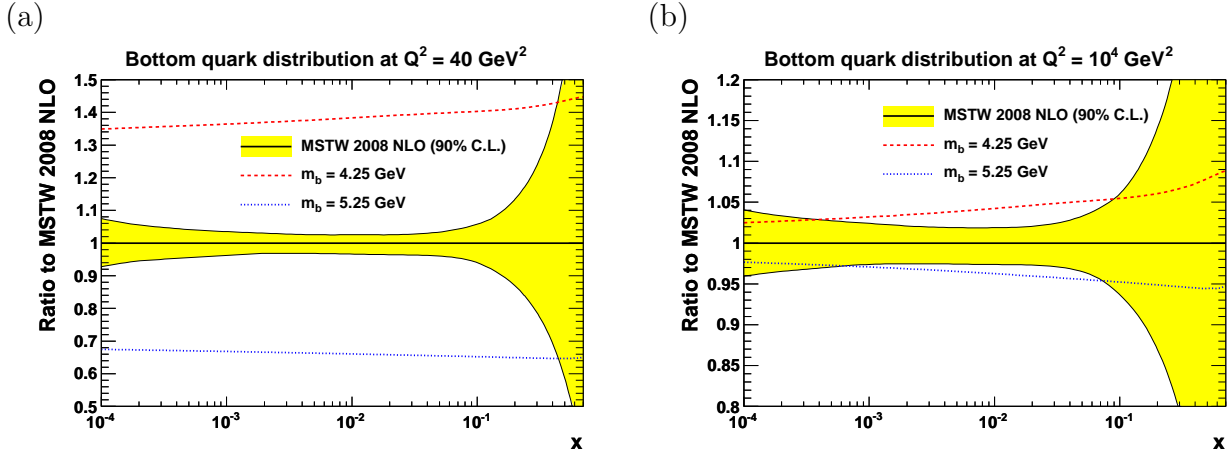


Figure 6: m_b dependence of bottom-quark distribution at NLO at two different Q^2 values, (a) 40 GeV^2 and (b) 10^4 GeV^2 , compared to the 90% C.L. PDF uncertainties.

the global χ^2 . We see that the F_2^b data show a slight preference for $m_b \approx 4.75 \text{ GeV}$ at NLO and $m_b \approx 5.00 \text{ GeV}$ at NNLO. The global fits (including the F_2^b data, obtained by simply adding the χ^2 values), would prefer $m_b \approx 4.50\text{--}4.75 \text{ GeV}$ at NLO and $m_b \approx 4.50\text{--}5.00 \text{ GeV}$ at NNLO, although admittedly the χ^2 profiles are quite flat, see Table 2. We conclude that the global data do not meaningfully constrain m_b , and that, in view of Table 2 and Fig. 5, the choice $m_b = 4.75 \text{ GeV}$ made in the MSTW 2008 [1] analysis is completely satisfactory.

The dependence of the bottom-quark distribution on the value taken for m_b is shown in Fig. 6. The plots show the ratio of the NLO PDFs obtained with $m_b = 4.25 \text{ GeV}$ and $m_b = 5.25 \text{ GeV}$ to those of the MSTW 2008 analysis (which assumed $m_b = 4.75 \text{ GeV}$) at scales of $Q^2 = 40 \text{ GeV}^2$ and $Q^2 = 10^4 \text{ GeV}^2$. We see that the b -quark ratios lie well outside the 90% C.L. PDF uncertainty at $Q^2 = 40 \text{ GeV}^2$ and even at $Q^2 = 10^4 \text{ GeV}^2$. The gluon distribution and the other quark flavours are hardly affected by the value of m_b (not shown here).

3.3 Pole masses of heavy quarks

Note that in our analyses m_c refers to the *pole* mass of the charm quark. Both the transition matrix elements defining the boundary conditions for heavy-quark evolution [11] and the heavy-quark coefficient functions used to define the GM-VFNS [11] are defined using the on-shell renormalisation scheme for the heavy quark. Unlike $\alpha_S(\mu^2)$, the pole mass m_c is, in principle, a physically-defined (spoilt by confinement which gives power corrections, see below) quantity which is stable to the order of perturbation theory. So the values that we obtain in the NLO and NNLO analyses should, in principle, be the same. However, we see from Fig. 1 that the values are only marginally compatible. This is due to a variety of reasons. The perturbative expansion of heavy-flavour coefficient functions is not as convergent as one might hope, with large corrections near threshold and in the small- x limit. So even though the pole mass might, in principle, be the same quantity at two different perturbative orders, the calculation at lower

orders is missing significant corrections at higher orders which will affect the value of the pole mass obtained in an extraction from data. Perhaps most important in this respect is the large negative boundary condition (at $Q^2 = m_h^2$) for the heavy-flavour distribution at NNLO, which has the effect of flattening the slope $\partial F_2^h / \partial \ln Q^2$ (see Ref. [14] for details) and implies a lower mass to correct for this. There is also more potential variation in the GM-VFNS definition at NLO than NNLO, and there would be slightly more stability in preferred pole mass in, for example, the “optimal” scheme introduced in Ref. [64] (although this does not remove the variation and is the subject for a future study). Finally, as briefly noted above and discussed further below, the definition of the pole mass is contaminated by non-perturbative corrections. These are reflected in the divergence of the perturbation theory and power corrections are, in practice, difficult to disentangle from higher-order corrections, so extractions at different orders will have a variation from this source. We now examine this issue in more detail.

Let us consider the values we extract and use as default. In the *Review of Particle Physics* [65], the authors quote values for the “running” masses, $m_c(\mu = m_c)$ and $m_b(m_b)$, in the $\overline{\text{MS}}$ scheme:

$$m_c(\mu = m_c) = 1.27^{+0.07}_{-0.11} \text{ GeV}, \quad m_b(m_b) = 4.20^{+0.17}_{-0.07} \text{ GeV}, \quad (6)$$

which they evaluate from a whole series of independent determinations. This implies a precise determination of masses.⁶ The best precision of the pole mass should be obtained by using this $\overline{\text{MS}}$ value (the best determinations coming from NNNLO calculations) with the most accurate conversion factor, also at NNNLO. However, the conversion of the “running” mass to the pole mass is problematic, since it relies on a very weakly convergent perturbative expansion. Using our NNLO value of α_S , the term-by-term conversion factor (obtained from the formula in Ref. [65]), starting at zeroth order and going to the highest known order of α_S^3 [68, 69], for the bottom-quark mass is $(1 + 0.095 + 0.045 + 0.036)$ and for charm is $(1 + 0.16 + 0.14 + 0.18)$.⁷ The former implies that convergence is ceasing, while the latter has no real convergence at all, since it relies on a much higher value of α_S (and larger coefficients due to less cancellation between individual terms as the number of light quark flavours decreases [68, 69]).

Indeed, the contamination by renormalons of the perturbative series for the transformation of a running quark mass in the $\overline{\text{MS}}$ scheme to the pole mass has been known for a long time [71, 72]. These papers estimate the intrinsic ambiguity of the perturbative series due to infrared contributions, translating into an uncertainty on the pole mass of at least 0.05 GeV, but more likely of order 0.1–0.2 GeV. The best estimate one can obtain from the perturbative series

⁶There are numerous individual determinations of both charm- and bottom-quark masses in the $\overline{\text{MS}}$ scheme which are actually even more precise than the above—for recent examples see Refs. [66, 67]. However, these can vary from each other by considerably more than the quoted uncertainties, so in the *Review of Particle Physics* [65] account is taken of the spread, as well as the individual uncertainties.

⁷Use of an NNNLO value of α_S would make little difference. As shown in Ref. [70], NNNLO extractions of $\alpha_S(M_Z^2)$ are very similar to the corresponding NNLO values, and the slightly quicker running at NNNLO would marginally increase α_S at the scale of the charm- and bottom-quark masses, i.e. the convergence of the perturbative series would likely be very slightly worse.

is usually defined by including all terms in the series until they cease to fall in magnitude from one order to the next. For the bottom quark, under the plausible assumption that the unknown $\mathcal{O}(\alpha_s^4)$ term is similar in size to the calculated $\mathcal{O}(\alpha_s^3)$ term, this would give a pole mass of $m_b = 4.9$ GeV. The uncertainty on this value from the conversion is either the estimate from Ref. [72] or roughly the size of the last term included in the series, i.e. 0.15 GeV. The good correspondence of the two estimates of the uncertainty is expected, and suggests that the series is indeed truncated at the correct point. If this uncertainty is added (approximately) in quadrature with the uncertainty on the $\overline{\text{MS}}$ scheme mass, Eq. (6), we obtain $m_b = 4.9 \pm 0.2$ GeV.

The determination of the charm-quark pole mass by conversion from the $\overline{\text{MS}}$ scheme mass is more problematic since, as noted above, the perturbative series displays no clear convergence at all. However, as discussed in Ref. [73], the leading renormalon contribution is the same for different masses, i.e. $\delta m^2 \propto \Lambda_{\text{QCD}}^2$, independent of quark flavour. This means the difference between m_b and m_c can be well determined, and turns out to be 3.4 GeV with a very small uncertainty [73]. Using this result we obtain a best determination of the charm-quark pole mass of $m_c = 1.5 \pm 0.2$ GeV. There is an uncertainty on $m_b - m_c$ due to the fact that the non-dominant renormalon contributions, $\delta m^2 \propto \Lambda_{\text{QCD}}^4/m^2$ and beyond, do not cancel. However, the uncertainty on $m_b - m_c$ is small compared to the 0.2 GeV uncertainty on m_b and hence does not affect the uncertainty on m_c at the quoted accuracy when added in quadrature.

These pole mass values obtained from $\overline{\text{MS}}$ conversion:

$$m_c = 1.5 \pm 0.2 \text{ GeV}, \quad m_b = 4.9 \pm 0.2 \text{ GeV}, \quad (7)$$

are slightly high compared with our default values (1.4 GeV and 4.75 GeV) and our best-fit values of m_c , particularly at NNLO, but even in the most discrepant case the error bars overlap. Combining our best-fit m_c values and the pole mass determination given in Eq. (7), it seems that a range for m_c of about 1.25–1.55 GeV at 68% C.L. and 1.15–1.65 GeV at 90% C.L. would seem reasonable at present. With improved HERA data on F_2^c to come [74] this range can hopefully be narrowed in the near future. Turning now to the bottom mass, the limited information that we obtain from comparison to data, and from the determination of the pole mass given in Eq. (7), suggest that a range of m_b from about 4.65–5.05 GeV at 68% C.L. would seem sensible. As we will see in the next section, LHC cross sections that do not involve explicit b -quarks are not very sensitive to the PDF variation with m_b , so using our grids at 4.5 and 5 GeV should give a good estimate of the uncertainty due to m_b at 68% C.L., and the grids at 4.25 and 5.25 GeV should give a conservative estimate of this source of uncertainty at 90% C.L. As with charm, improved HERA data on F_2^b are likely to limit the allowed spread in future.

If we reach the stage where we become confident that the data are starting to constrain the pole masses to an accuracy clearly better than the renormalon ambiguity, it may become preferable to transform to a scheme where $\overline{\text{MS}}$ definitions are used instead, even though the mass is less directly related to a physical variable in this case. This would be appropriate if we become strongly constrained by data with $Q^2 \sim m_h^2$ and data close to the kinematic threshold, $W^2 = Q^2(1/x - 1) = 4m_h^2$ (for neutral-current DIS), where non-perturbative effects

and the interplay between the leading-twist power-series and the power corrections become very important, and the ambiguities may be reduced in a different renormalisation scheme. Indeed, we have already noted in Section 9.2 of Ref. [1] that the lowest- Q^2 EMC data on F_2^c [75] imply a non-perturbative correction to the cross section.

3.4 Impact on W , Z and Higgs production at the Tevatron and LHC

Tables 3 and 4 show how the predictions for the “standard candle” NNLO W and Z cross sections at the Tevatron and LHC change using the PDFs obtained when the charm- and bottom-quark masses are varied in the global fit. The cross sections are calculated in the 5-flavour ZM-VFNS as described in Section 15 of Ref. [1], e.g. using the PDG 2008 [65] electroweak parameters. These changes are not due primarily to the changes in the heavy-quark PDFs themselves, which would in any case be in the opposite direction. Rather they are due to the changes in the light quarks, which evolve slightly more rapidly at small x to compensate for the slower turn-on of the heavy-flavour contribution to the structure functions when the heavy-quark masses are increased. In the free coupling case this is achieved mainly by an increase in α_S , while for fixed coupling it occurs from an increase in the small- x input gluon distribution. Additionally, the input sea quarks, mainly the less well-constrained strange quark distributions, also increase with increasing m_h to compensate for the suppressed heavy-flavour contribution to small- x structure functions. At the Tevatron, varying the charm mass by ± 0.15 GeV from its default MSTW 2008 value leads to fairly small ($\mathcal{O}(1\%)$ or less) changes in the W and Z cross sections, with heavier values of the charm mass giving slightly larger cross sections. The effects are a little more pronounced at the LHC: the cross sections vary by about $\pm 2\%$ for $\sqrt{s} = 14$ TeV. These changes reflect the behaviour of the up-quark distribution shown in Fig. 7(a) at the relevant x values (indicated). The sensitivity to the value of m_c of the W and Z cross sections at the LHC has previously been noticed in Ref. [76].

In Tables 3 and 4 we also give the changes to the cross section for the production via gluon-gluon fusion through a top-quark loop of a Standard Model Higgs boson of mass 120 GeV, calculated in the 5-flavour ZM-VFNS as described in Section 6.2 of Ref. [6]. From Table 3 we see that the variation of the Higgs cross sections with m_c is different depending on whether α_S is (a) allowed to vary or (b) kept fixed. This can be understood from the behaviour of the gluon distribution as m_c is varied, see Fig. 7(b). When α_S is fixed, the change in the Higgs cross section reflects the change in the gluon distribution at the relevant x values (indicated). Thus the {14 TeV LHC, 7 TeV LHC, Tevatron} Higgs cross sections are {correlated, uncorrelated, anticorrelated} with m_c . On the other hand, for variable α_S , the additional correlation of α_S with m_c (see Table 1) results in {14 TeV LHC, 7 TeV LHC, Tevatron} Higgs cross sections that are {correlated, correlated, almost uncorrelated} with m_c , i.e. at the Tevatron the anticorrelation of the gluon distribution largely cancels the correlation of α_S .

From Table 4 we see that the W , Z and Higgs production cross sections are much less dependent on the value of m_b . As seen from Table 2, the correlation between m_b and $\alpha_S(M_Z^2)$

(a)

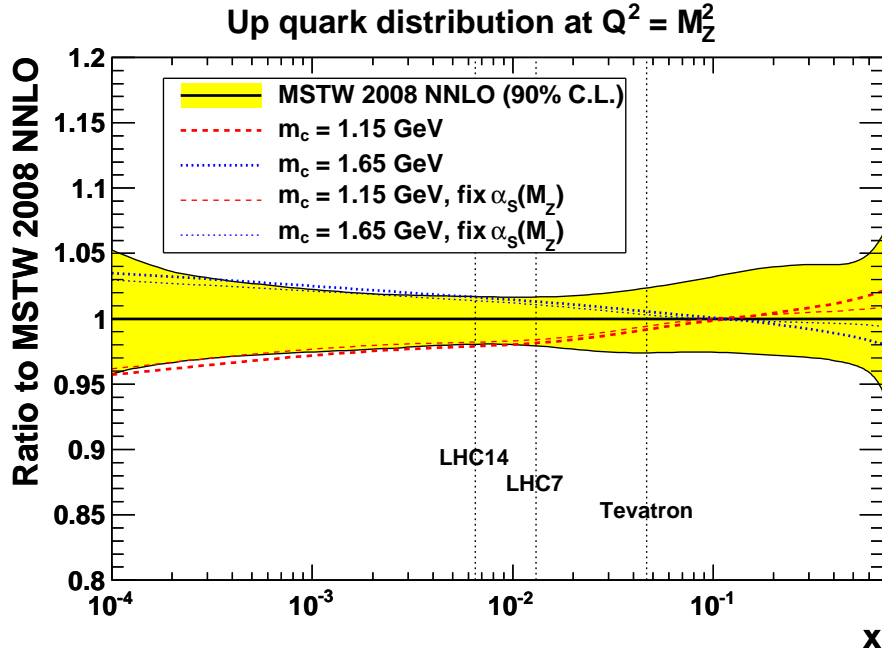
Variable $\alpha_S(M_Z^2)$		Tevatron ($\sqrt{s} = 1.96$ TeV)			LHC ($\sqrt{s} = 7$ TeV)			LHC ($\sqrt{s} = 14$ TeV)		
m_c (GeV)	m_b (GeV)	$\delta\sigma^W$	$\delta\sigma^Z$	$\delta\sigma^H$	$\delta\sigma^W$	$\delta\sigma^Z$	$\delta\sigma^H$	$\delta\sigma^W$	$\delta\sigma^Z$	$\delta\sigma^H$
1.05	4.75	-2.6	-2.8	+0.4	-4.1	-4.6	-2.4	-5.1	-5.5	-3.8
1.10		-2.2	-2.4	+0.2	-3.5	-3.9	-2.1	-4.3	-4.7	-3.3
1.15		-1.8	-1.9	+0.1	-2.9	-3.3	-1.8	-3.6	-3.9	-2.8
1.20		-1.4	-1.5	+0.1	-2.3	-2.6	-1.5	-2.8	-3.1	-2.3
1.25		-1.0	-1.1	0.0	-1.7	-1.9	-1.2	-2.1	-2.3	-1.7
1.30		-0.7	-0.7	0.0	-1.1	-1.3	-0.8	-1.4	-1.5	-1.2
1.35		-0.3	-0.4	0.0	-0.6	-0.6	-0.4	-0.7	-0.8	-0.6
1.40		0.0	0.0	0.0	0.0	0.0	0.0	0.0	0.0	0.0
1.45		+0.3	+0.3	0.0	+0.6	+0.6	+0.4	+0.7	+0.8	+0.6
1.50		+0.6	+0.6	0.0	+1.1	+1.3	+0.8	+1.3	+1.5	+1.2
1.55		+0.8	+0.9	+0.1	+1.6	+1.9	+1.2	+2.0	+2.3	+1.8
1.60		+1.1	+1.2	+0.2	+2.1	+2.5	+1.8	+2.6	+3.0	+2.5
1.65		+1.3	+1.5	+0.1	+2.6	+3.0	+2.0	+3.2	+3.7	+2.9
1.70		+1.5	+1.8	+0.2	+3.1	+3.6	+2.5	+3.8	+4.4	+3.6
1.75		+1.8	+2.0	+0.3	+3.5	+4.2	+2.9	+4.3	+5.1	+4.1

(b)

Fixed $\alpha_S(M_Z^2)$		Tevatron ($\sqrt{s} = 1.96$ TeV)			LHC ($\sqrt{s} = 7$ TeV)			LHC ($\sqrt{s} = 14$ TeV)		
m_c (GeV)	m_b (GeV)	$\delta\sigma^W$	$\delta\sigma^Z$	$\delta\sigma^H$	$\delta\sigma^W$	$\delta\sigma^Z$	$\delta\sigma^H$	$\delta\sigma^W$	$\delta\sigma^Z$	$\delta\sigma^H$
1.05	4.75	-1.9	-2.2	+3.8	-2.9	-3.4	0.0	-3.9	-4.3	-1.5
1.10		-1.5	-1.8	+3.3	-2.5	-2.9	0.0	-3.3	-3.6	-1.3
1.15		-1.2	-1.4	+2.7	-2.1	-2.4	0.0	-2.7	-3.0	-1.1
1.20		-0.9	-1.1	+2.2	-1.6	-1.9	0.0	-2.1	-2.4	-0.9
1.25		-0.7	-0.8	+1.6	-1.2	-1.4	0.0	-1.6	-1.8	-0.7
1.30		-0.4	-0.5	+1.1	-0.8	-1.0	0.0	-1.0	-1.2	-0.4
1.35		-0.2	-0.3	+0.5	-0.4	-0.5	0.0	-0.5	-0.6	-0.2
1.40		0.0	0.0	0.0	0.0	0.0	0.0	0.0	0.0	0.0
1.45		+0.2	+0.2	-0.6	+0.4	+0.5	0.0	+0.5	+0.6	+0.3
1.50		+0.3	+0.4	-1.2	+0.8	+0.9	0.0	+1.0	+1.2	+0.4
1.55		+0.5	+0.7	-1.7	+1.1	+1.4	0.0	+1.4	+1.7	+0.6
1.60		+0.7	+0.8	-2.3	+1.4	+1.8	0.0	+1.9	+2.2	+0.9
1.65		+0.8	+1.1	-2.9	+1.8	+2.3	-0.1	+2.3	+2.8	+1.0
1.70		+0.9	+1.2	-3.5	+2.1	+2.7	-0.1	+2.7	+3.3	+1.2
1.75		+1.1	+1.4	-4.0	+2.4	+3.1	-0.1	+3.1	+3.8	+1.3

Table 3: (a) Difference (in percent) between the predictions for the W , Z and Standard Model Higgs ($M_H = 120$ GeV) NNLO production cross sections at the Tevatron and LHC, calculated using the variable- m_c PDF sets, and the standard MSTW 2008 NNLO predictions with $m_c = 1.40$ GeV. (b) Also shown are the corresponding results for variable m_c with *fixed* $\alpha_S(M_Z^2)$.

(a)



(b)

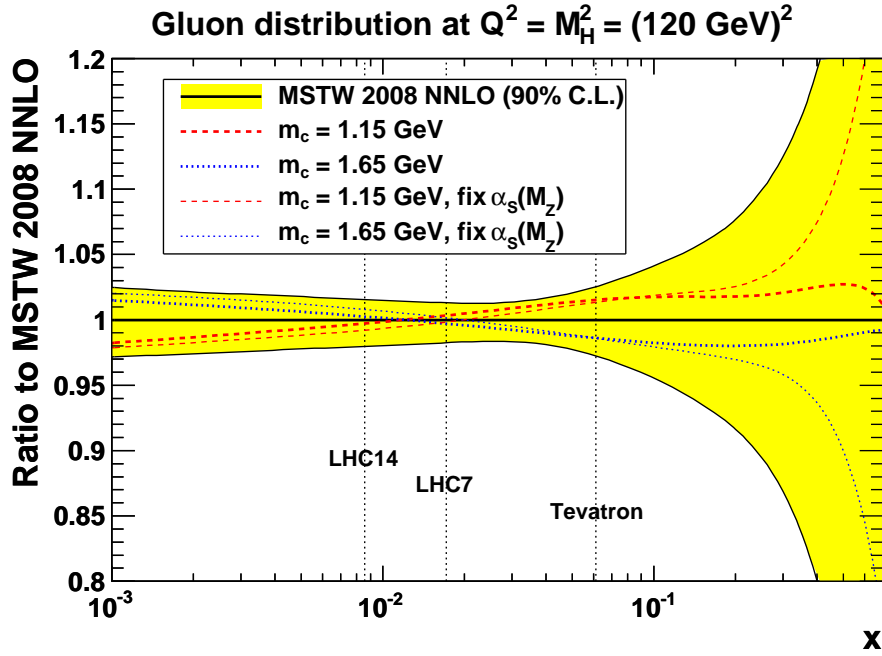


Figure 7: m_c dependence of the NNLO (a) up-quark and (b) gluon distributions at the scales relevant for Z and Higgs boson ($M_H = 120 \text{ GeV}$) production, respectively. Also shown is the m_c dependence when $\alpha_s(M_Z^2)$ is held fixed. The values of $x = M_{Z,H}/\sqrt{s}$ probed at central rapidity (and $p_T^{Z,H} = 0$) are indicated for the Tevatron ($\sqrt{s} = 1.96 \text{ TeV}$) and LHC (7 TeV and 14 TeV).

Variable $\alpha_S(M_Z^2)$		Tevatron ($\sqrt{s} = 1.96$ TeV)			LHC ($\sqrt{s} = 7$ TeV)			LHC ($\sqrt{s} = 14$ TeV)		
m_c (GeV)	m_b (GeV)	$\delta\sigma^W$	$\delta\sigma^Z$	$\delta\sigma^H$	$\delta\sigma^W$	$\delta\sigma^Z$	$\delta\sigma^H$	$\delta\sigma^W$	$\delta\sigma^Z$	$\delta\sigma^H$
1.40	4.00	-0.2	-0.1	-0.2	-0.4	-0.1	-0.4	-0.5	0.0	-0.5
	4.25	-0.1	-0.1	-0.1	-0.3	0.0	-0.3	-0.3	0.0	-0.3
	4.50	-0.1	0.0	-0.1	-0.1	0.0	-0.1	-0.1	0.0	-0.1
	4.75	0.0	0.0	0.0	0.0	0.0	0.0	0.0	0.0	0.0
	5.00	0.0	0.0	0.0	+0.1	0.0	+0.1	+0.1	0.0	+0.1
	5.25	+0.1	0.0	+0.1	+0.2	0.0	+0.2	+0.2	0.0	+0.2
	5.50	+0.1	0.0	+0.1	+0.3	0.0	+0.2	+0.3	-0.1	+0.3

Table 4: Difference (in percent) between the predictions for the W , Z and Standard Model Higgs ($M_H = 120$ GeV) NNLO production cross sections at the Tevatron and LHC, calculated using the variable- m_b PDF sets, and the standard MSTW 2008 NNLO predictions with $m_b = 4.75$ GeV. Here $\alpha_S(M_Z^2)$ is a free parameter in each fit, although the correlation with m_b is negligible, see Table 2.

is negligible, so we do not explicitly show results with fixed $\alpha_S(M_Z^2)$ since they would be almost the same as in Table 4. In all cases, for both varying- m_c and varying- m_b , the cross-section ratios σ^W/σ^Z (and also $\sigma^{W^+}/\sigma^{W^-}$ at the LHC) are almost completely unaffected.

In order to assess the *total* uncertainty on a hadron collider cross section arising from variations in PDFs, α_S and the heavy-quark masses, we need to define a prescription for combining the latter with the former. Our recommendation is to vary m_c in the range $m_c = 1.40 \pm 0.15$ GeV at 68% C.L. and ± 0.25 GeV at 90% C.L., centred on the default value for fixed α_S , and to vary m_b in the range $m_b = 4.75 \pm 0.25$ GeV at 68% C.L. and ± 0.50 GeV at 90% C.L., and then to separately add the resulting cross-section variations in quadrature with the usual ‘‘PDF+ α_S ’’ uncertainty. Of course, this prescription does not account for all possible correlations between PDFs, α_S and $m_{c,b}$, but it should be a sufficiently good approximation. The range of m_c values is based on the slightly contrasting pulls of the pole mass determination from the $\overline{\text{MS}}$ conversion and our fit. As an example, in Table 5 we show the increase in uncertainty on the W , Z and Higgs total cross sections due to m_c and m_b variations, compared to the ‘‘PDF only’’ [1] and ‘‘PDF+ α_S ’’ [6] uncertainties.

In Table 6 we compare the values of the heavy-quark masses, m_c and m_b , used in the MRST/MSTW analyses, with the values taken in the most recent public PDF fits of other groups. The other two *global* PDF fitting groups, CTEQ [3,4] and NNPDF [5], do not attempt to quantify the uncertainty coming from $m_{c,b}$, neither do the fits of ‘‘dynamical’’ PDFs by GJR/JR [77,78]. The HERAPDF1.0 fit [79] uses the same central values as MSTW08 [1], but additional PDF fits are also provided with $m_c = \{1.35, 1.65\}$ GeV and $m_b = \{4.3, 5.0\}$ GeV, and this additional model uncertainty is recommended to be added in quadrature with the other uncertainties. The ABKM09 analysis [80] uses fixed values of $m_c = 1.5$ GeV and $m_b = 4.5$ GeV to determine the central fit. However, additional pseudo-measurements of $m_{c,b}$ are then added, with values given in the last line of Table 6, and m_c and m_b are taken as free parameters to calculate the covariance matrix used for the final error propagation. This means that each of

Tevatron, $\sqrt{s} = 1.96$ TeV			
	$B_{\ell\nu} \cdot \sigma^W$	$B_{\ell^+\ell^-} \cdot \sigma^Z$	σ^H
Central value	2.747 nb	0.2507 nb	0.9550 pb
PDF only uncertainty	+1.8%	+1.9%	+3.1%
	-1.5%	-1.6%	-3.3%
PDF+ α_S uncertainty	+2.2%	+2.2%	+5.4%
	-1.7%	-1.8%	-4.8%
PDF+ $\alpha_S+m_{c,b}$ uncertainty	+2.3%	+2.3%	+5.6%
	-1.8%	-2.0%	-5.1%
LHC, $\sqrt{s} = 7$ TeV			
	$B_{\ell\nu} \cdot \sigma^W$	$B_{\ell^+\ell^-} \cdot \sigma^Z$	σ^H
Central value	10.47 nb	0.958 nb	15.50 pb
PDF only uncertainty	+1.7%	+1.7%	+1.1%
	-1.6%	-1.5%	-1.6%
PDF+ α_S uncertainty	+2.5%	+2.5%	+3.7%
	-1.9%	-1.9%	-2.9%
PDF+ $\alpha_S+m_{c,b}$ uncertainty	+2.7%	+2.9%	+3.7%
	-2.2%	-2.4%	-2.9%
LHC, $\sqrt{s} = 14$ TeV			
	$B_{\ell\nu} \cdot \sigma^W$	$B_{\ell^+\ell^-} \cdot \sigma^Z$	σ^H
Central value	21.72 nb	2.051 nb	50.51 pb
PDF only uncertainty	+1.7%	+1.7%	+1.0%
	-1.7%	-1.6%	-1.6%
PDF+ α_S uncertainty	+2.6%	+2.6%	+3.6%
	-2.2%	-2.1%	-2.7%
PDF+ $\alpha_S+m_{c,b}$ uncertainty	+3.0%	+3.1%	+3.7%
	-2.7%	-2.8%	-2.8%

Table 5: NNLO predictions for W , Z and Higgs ($M_H = 120$ GeV) total cross sections at the Tevatron, 7 TeV LHC and 14 TeV LHC, with PDF uncertainties only [1], with the combined “PDF+ α_S ” uncertainty [6], then finally also including the uncertainty due to m_c and m_b . The 68% C.L. uncertainties are given in all cases. We take $\mu_R = \mu_F = M_{W,Z,H}$.

PDF set	m_c (GeV)	m_b (GeV)
MSTW08 [1, this work]	1.40 ± 0.15	4.75 ± 0.25
MRST06 [2]	1.43	4.30
CT10 [3]	1.30	4.75
CTEQ6.6 [4]	1.30	4.50
NNPDF2.0 [5]	$\sqrt{2}$	4.30
GJR08/JR09 [77, 78]	1.30	4.20
HERAPDF1.0 [79]	$1.40^{+0.20}_{-0.05}$	$4.75^{+0.25}_{-0.45}$
ABKM09 [80]	1.50 ± 0.10	4.50 ± 0.50

Table 6: Values of m_c and m_b used in various PDF fits. The 1σ uncertainties are given only for the three PDF groups who attempt to account for uncertainties on $m_{c,b}$ in their analyses.

the public eigenvector PDF sets will be associated with different values of m_c and m_b , but these values are not readily accessible.

4 3-flavour and 4-flavour scheme parton distributions

As well as looking at the variation in the parton distributions as a function of the heavy-quark masses, it is also interesting to consider the PDF sets obtained in the framework of a different maximum number of active quark flavours. Hence, in this section we will consider our PDFs when charm becomes an active parton but bottom does not—the 4-flavour scheme—and when both the charm and bottom quarks only appear in the final state—the 3-flavour scheme. We have argued on various occasions (e.g. in Section 4 of Ref. [1]) that the use of a GM-VFNS, i.e. with up to five active quarks (or even six if we include top), is preferable. However, there are cases where the cross section has only been calculated with finite mass dependence for the fixed flavour number case; see, for example, the HQVDIS program [19, 20] for details of final states in heavy-quark production in DIS. For this reason we make available sets of 3FS and 4FS distributions with a variety of both charm and bottom masses.

4.1 Obtaining 3-flavour and 4-flavour scheme parton distributions

It might be thought preferable to obtain these lower active quark number PDF sets from a fit performed using FFNS scheme coefficient functions. However, as argued in Refs. [9, 81], it is not actually so obvious that this is the case. This is largely because rather few of the data sets included in a truly global PDF fit can be kept, even at NLO, in a fit using the FFNS, due to lack of the full coefficient functions (even charged-current DIS coefficients are not known with full mass dependence at order α_S^2 except for $Q^2 \gg m_h^2$ [82]). Hence, the central values of the PDFs are likely to be influenced as much by the lack of data as by the change of scheme. However, it is also a consideration that the lack of resummation of the large logarithms in Q^2/m_h^2 potentially affects the stability of the fit compared to the presumably more stable GM-VFNS fit. Ultimately a correct GM-VFNS will provide results very similar to the FFNS near to the transition points $Q^2 = m_h^2$ anyway, so we deem it best to simply obtain the 3FS and 4FS PDFs from the inputs for the full fits performed using the GM-VFNS.

When obtaining the 3FS and 4FS PDFs it is vital to make a self-consistent definition of the strong coupling constant α_S . It is generally the case that coefficient functions calculated in the 3- or 4-flavour schemes are made in a renormalisation scheme where the contribution of the heavy quark decouples and the coupling itself does not include the heavy quark as an active flavour. On this basis we define the PDFs using this definition of the coupling in the splitting functions. It is certainly possible to use a different definition of the coupling, but this must be applied universally, in both the PDFs and the coefficient functions. As illustrated in Ref. [9], the error, made from not doing so, can be a few percent. Indeed, the change in the coupling

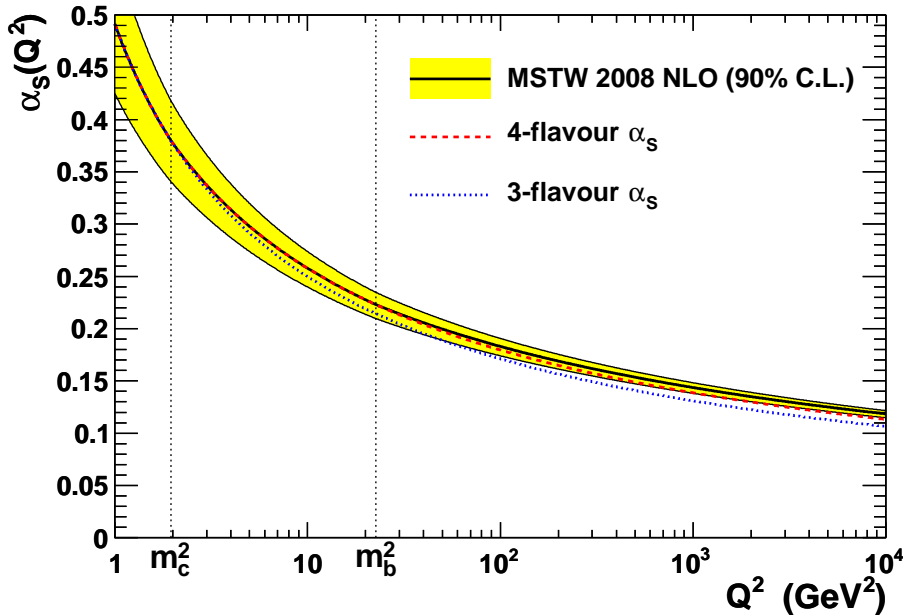
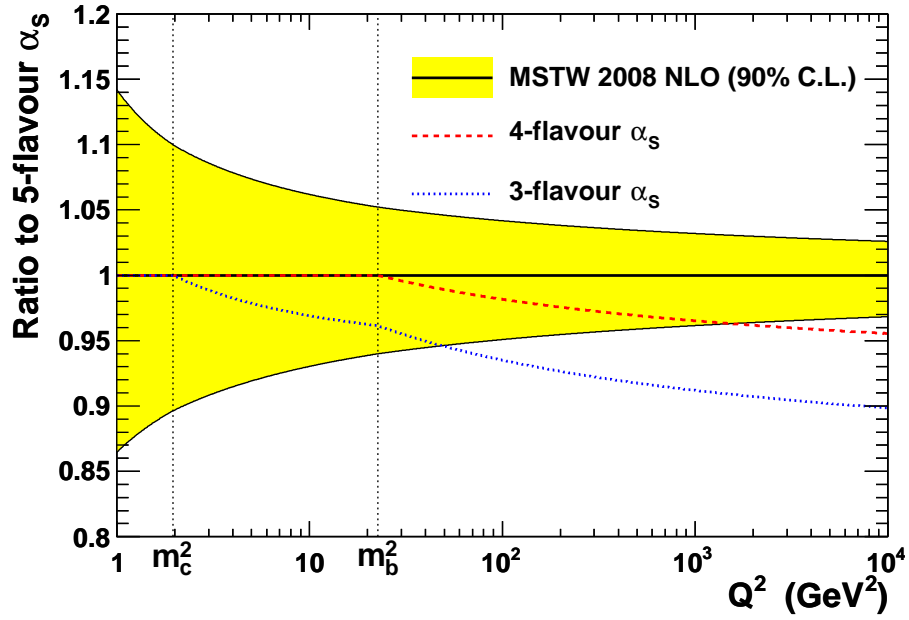


Figure 8: The NLO strong coupling $\alpha_S(Q^2)$ versus Q^2 , in the default 5FS with the 90% C.L. experimental uncertainty, and in the 4FS and 3FS, taking the same input value of $\alpha_S(Q_0^2 = 1 \text{ GeV}^2)$.

obtained by altering the number of heavy flavours is quite dramatic. In our default NLO fit we start with a value $\alpha_S(Q_0^2) = 0.49128$ (with $Q_0^2 = 1 \text{ GeV}^2$), which for a variable flavour number results in $\alpha_S^{(5)}(M_Z^2) = 0.12018$. Restricting ourselves to a maximum of four active flavours, the same boundary condition at Q_0^2 gives $\alpha_S^{(4)}(M_Z^2) = 0.11490$, and for three active flavours gives $\alpha_S^{(3)}(M_Z^2) = 0.10809$. This is illustrated in Fig. 8, and more clearly in Fig. 9(a), which shows the ratio of the 3- and 4-flavour α_S to the 5-flavour one.

We make available both the 3FS and 4FS NLO PDF sets for the full variety of fits with varying charm and bottom masses discussed in the previous section, including the case of varying m_c with fixed $\alpha_S(M_Z^2)$. We do not vary the quark mass at LO since the quality of the fit is already poor at LO. However, we do provide the 3FS and 4FS PDFs for the default masses at LO since these may be useful in some Monte Carlo event generators. We also make available the full range of 3FS and 4FS sets at NNLO, although the application of these is distinctly limited at present due to the lack of cross sections with full mass dependence calculated at this order. We will comment more on this in the following section. The ratios of the 3FS and 4FS NLO PDFs to those in the 5FS are shown in Fig. 10 at $Q^2 = 10^4 \text{ GeV}^2$. In both cases, the gluon is larger in the 4FS and, particularly, in the 3FS, due to the fact that it splits into a smaller number of quark–antiquark pairs; see also Fig. 9(b). The effect of the increased growth of the gluon distribution is countered exactly for the leading term in $\alpha_S(Q^2) \ln(Q^2/m_h^2)$ by the quicker decrease of the coupling. This is illustrated in Fig. 9, where the change in the gluon distribution comparing different flavour numbers is, to a good approximation, the inverse of

(a)



(b)

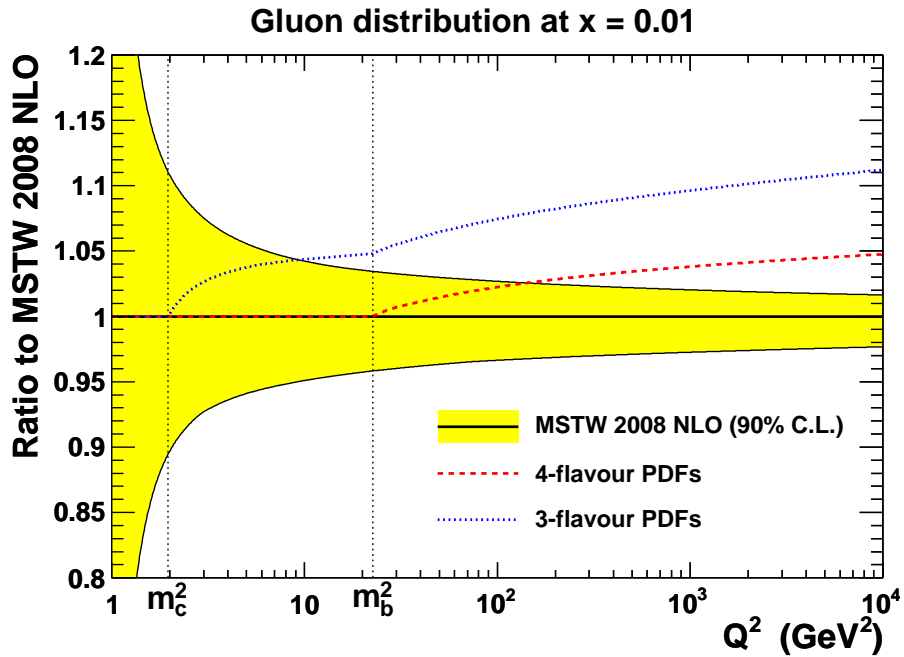


Figure 9: Ratio to the 5FS values of (a) strong coupling α_s and (b) gluon distribution at $x = 0.01$, versus Q^2 at NLO in the 4FS and 3FS, compared to the 90% C.L. experimental uncertainty bands.

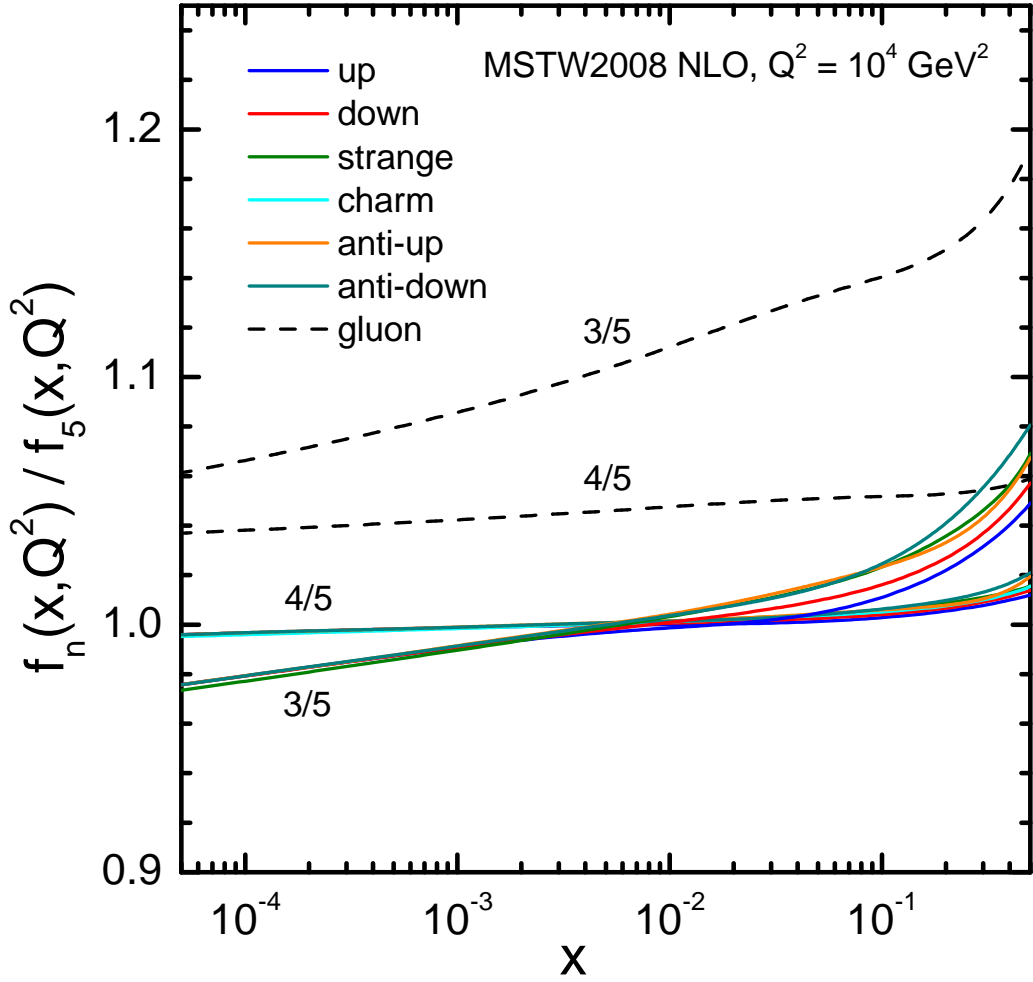


Figure 10: Ratio of 3FS and 4FS NLO PDFs to the standard 5FS NLO PDFs, at $Q^2 = 10^4 \text{ GeV}^2$.

that for α_S . This behaviour is only violated by higher-order corrections, so the gluon-driven change in the light quarks at small x is rather minimal. At higher x , the onset of the smaller coupling in the lower flavour number schemes means a slower evolution and consequently larger light-quark distributions, as seen in Fig. 10.

Finally, we also make available new eigenvector PDF sets for the 3- and 4-flavour PDFs using the default quark masses at LO, NLO and NNLO. These are evolved from the saved PDF parameters at $Q_0^2 = 1 \text{ GeV}^2$ for the default MSTW fits, i.e. the ‘‘dynamical’’ tolerance values, $T = (\Delta\chi_{\text{global}}^2)^{1/2}$, are those determined from the 5-flavour fit [1]. For the first time, this will allow PDF uncertainties to be consistently included in a 3FS or 4FS calculation. We have not yet generated the additional eigenvector PDF sets with varying α_S values needed for the ‘‘PDF+ α_S ’’ uncertainty calculation [6], although these could be provided at a future point if necessary. Note, however, that 3FS or 4FS calculations generally have large higher-order corrections, and an associated large (renormalisation and factorisation) scale dependence, which is common in processes with multiple hard scales. The theory uncertainty due to neglected higher-order corrections is therefore likely to dominate over any PDF or ‘‘PDF+ α_S ’’ uncertainty. Precise calculations of the latter quantities are therefore relatively less important than in typical 5FS calculations where higher-order corrections are more readily available.

4.2 Comparison of Z total cross-section predictions in 4FS and 5FS

We have already noted in Section 2 that while the parton distributions of a n FS, with appropriate coefficient functions, can give an adequate description of the production of an $(n + 1)$ th parton near threshold, the accuracy of the perturbative expansion becomes increasingly unreliable as the scale of the hard scattering process, Q^2 , increases above m_h^2 . In this section we illustrate this by considering the total Z cross section at hadron colliders. In particular, we compare the cross-section predictions in the 5FS (\equiv MSTW 2008 [1]) and 4FS defined previously. Since in this case $Q^2 = M_Z^2 \gg m_b^2$, we would expect to see quantitative differences between the predictions due to the resummed $[\alpha_S \log(M_Z^2/m_b^2)]^n$ terms which are implicit in the 5FS, via the evolution of the b -quark PDF and $\alpha_S^{(5)}$, but absent from the 4FS. For reasons which will become apparent below, we consider the Z cross section at both NLO and NNLO.

In the 4FS the b quarks are not considered as partons in the initial state, but contribute to the Z cross section via real and virtual contributions which first appear at $\mathcal{O}(\alpha_S^2)$ in perturbation theory. Therefore the only difference in the predicted cross sections at NLO are (i) explicit b -parton contributions $b + \bar{b} \rightarrow Z(+g)$ and $g + b(\bar{b}) \rightarrow Z + b(\bar{b})$ which only contribute in the $n_f = 5$ scheme (5FS), (ii) small differences in the light-quark and gluon distributions arising from the slightly different evolution in the two schemes, see Fig. 10, and (iii) the difference in the values of $\alpha_S^{(4)}(M_Z^2)$ and $\alpha_S^{(5)}(M_Z^2)$, see Figs. 8 and 9(a), which affect the size of the NLO K -factor. We would expect the Tevatron Z cross sections to be more similar than those at the LHC, since the b -quark contributions to the 5FS cross section are much smaller at the lower collider energy. We do not explicitly include PDF and/or α_S uncertainties on the calculated cross sections, as

Tevatron, $\sqrt{s} = 1.96$ TeV	$B \cdot \sigma_{\text{NLO}}^Z(4\text{FS})$ (nb)	$B \cdot \sigma_{\text{NLO}}^Z(5\text{FS})$ (nb)	$B \cdot \sigma_{\text{NLO}}^Z(5\text{FS}, b)$ (nb)
σ_0^Z	0.1989	0.1990	0.0012
σ_1^Z	0.0413	0.0436	-0.0002
total	0.2402	0.2426	0.0010
<hr/>			
LHC, $\sqrt{s} = 7$ TeV	$B \cdot \sigma_{\text{NLO}}^Z(4\text{FS})$ (nb)	$B \cdot \sigma_{\text{NLO}}^Z(5\text{FS})$ (nb)	$B \cdot \sigma_{\text{NLO}}^Z(5\text{FS}, b)$ (nb)
σ_0^Z	0.7846	0.8023	0.0205
σ_1^Z	0.1206	0.1285	-0.0020
total	0.9052	0.9308	0.0185
<hr/>			
LHC, $\sqrt{s} = 14$ TeV	$B \cdot \sigma_{\text{NLO}}^Z(4\text{FS})$ (nb)	$B \cdot \sigma_{\text{NLO}}^Z(5\text{FS})$ (nb)	$B \cdot \sigma_{\text{NLO}}^Z(5\text{FS}, b)$ (nb)
σ_0^Z	1.6922	1.7545	0.0656
σ_1^Z	0.2303	0.2465	-0.0050
total	1.9225	2.0009	0.0601

Table 7: NLO predictions for the total Z cross section (multiplied by leptonic branching ratio B) at the Tevatron and LHC using MSTW 2008 NLO PDFs [1] as input, broken down into the α_S^n ($n = 0, 1$) contributions, with $\{q = u, d, s, c; \alpha_S^{(4)}; 4\text{-flavour MSTW 2008 NLO PDFs}\}$ in the 4FS calculation and $\{q = u, d, s, c, b; \alpha_S^{(5)}; 5\text{-flavour MSTW 2008 NLO PDFs}\}$ in the 5FS calculation. The final column gives the contribution to the 5FS cross sections from processes where the Z couples directly to b quarks.

these are presumed to be more or less the same for the 4FS and 5FS calculations. Contributions from top quarks are also not included, as these have been shown to be very small in Ref. [83], and in any case should be added to both the 4FS and 5FS cross sections.

The results at NLO are shown in Table 7.⁸ The 4FS cross section is smaller by 1.0%, 2.8% and 3.9% at the Tevatron, LHC(7 TeV) and LHC(14 TeV) respectively. The $\mathcal{O}(\alpha_S^1)$ contributions differ by more than the $\mathcal{O}(\alpha_S^0)$ contributions, due to the $\sim 5\%$ differences in the $\alpha_S(M_Z^2)$ values in the two schemes. Also shown in Table 7 (final column) are the contributions to the 5FS cross sections from the $b + \bar{b} \rightarrow Z(+g)$ and $g + b(\bar{b}) \rightarrow Z + b(\bar{b})$ processes, which evidently account for 0.4%, 2.0% and 3.0% of the total at the Tevatron, LHC(7 TeV) and LHC(14 TeV) respectively. Thus these contributions account for the bulk of the differences in the 4FS and 5FS cross sections at the LHC energies.

As noted above, when making a comparison between the 4FS and 5FS calculations at NNLO, we must include in the former the explicit real and virtual b -quark contributions which first appear at $\mathcal{O}(\alpha_S^2)$ in perturbation theory. When calculated with a non-zero b -quark mass⁹ these contributions are finite, and simply add to the 4-flavour contributions. Sample Feynman

⁸The 5FS cross sections are identical to those reported in Ref. [1].

⁹For consistency, we use $m_b = 4.75$ GeV, the same value used in the 5FS [1] to generate the b -quark PDFs via the DGLAP equation.

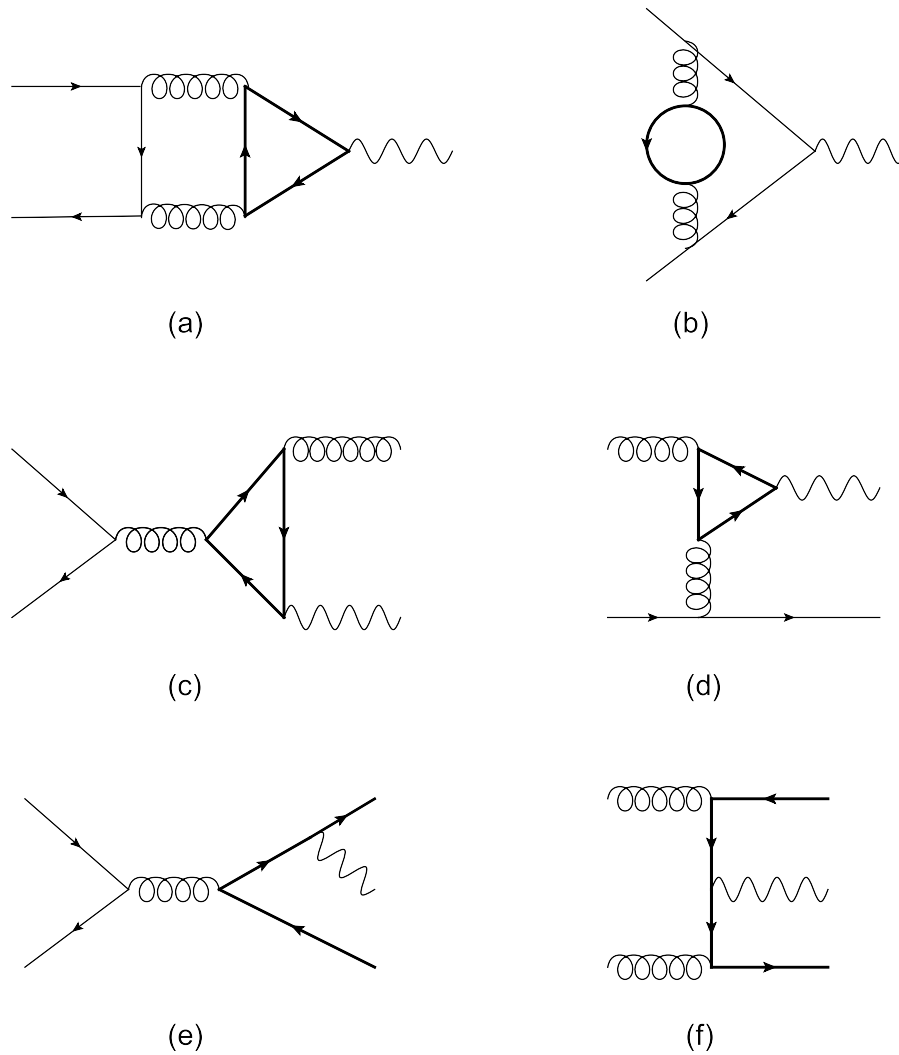


Figure 11: Sample Feynman diagrams for the various (a,b,c,d) virtual and (e,f) real b -quark contributions to the Z cross section. The b -quarks are shown as the thicker fermion lines.

subprocess	$\Delta_b \sigma^Z$ (Tevatron)	$\Delta_b \sigma^Z$ (LHC, 7 TeV)	$\Delta_b \sigma^Z$ (LHC, 14 TeV)
$q + \bar{q} \rightarrow Z$	5.230×10^{-6}	-2.124×10^{-5}	-6.440×10^{-5}
$q + \bar{q} \rightarrow Z + g$	4.901×10^{-5}	6.185×10^{-5}	9.701×10^{-5}
$q(\bar{q}) + g \rightarrow Z + q(\bar{q})$	-2.862×10^{-5}	-1.456×10^{-4}	-2.632×10^{-4}
$q + \bar{q} \rightarrow Z + b + \bar{b}$	3.754×10^{-4}	1.450×10^{-3}	3.382×10^{-3}
$g + g \rightarrow Z + b + \bar{b}$	2.090×10^{-4}	5.287×10^{-3}	1.997×10^{-2}
total	6.100×10^{-4}	6.632×10^{-3}	2.312×10^{-2}

Table 8: Additional $\mathcal{O}(\alpha_S^2)$ contributions to the total Z 4FS NNLO cross section in nb (multiplied by leptonic branching ratio) at the Tevatron and LHC arising from real and virtual b -quark processes.

diagrams for the various real and virtual b -quark contributions are shown in Fig. 11, and analytic expressions are given in Refs. [83,84]. We summarise these in Appendix A, and derive small-mass (i.e. $m_b^2/M_Z^2 \ll 1$) expansions which are useful in practice. The results are presented in Table 8, for Tevatron and ($\sqrt{s} = 7, 14$ TeV) LHC energies. Evidently the $2 \rightarrow 3$ process contributions, Eq. (A.7), are by far the most dominant, and especially so at the LHC where they are two orders of magnitude larger than the rest of the $\mathcal{O}(\alpha_S^2)$ contributions combined. In Table 9 we add these real and virtual b -quark contributions to the bulk of the NNLO cross section coming from 4FS light quarks and gluons, and compare the total with the benchmark 5FS NNLO results presented in Ref. [1], in which the b quark is treated as a massless parton in the subprocess cross sections, i.e. both in the initial and final states and in loop contributions. Also shown in Table 9 are the $(b\bar{b}, bg, \dots)$ contributions in which the Z couples directly to a b quark and in which there is at least one b or \bar{b} quark in the initial state.¹⁰ These represent 0.03%, 1.5% and 2.4% of the total 5FS NNLO cross sections at the Tevatron, LHC(7 TeV) and LHC(14 TeV) respectively.

From Table 9, we see that at the Tevatron the 5FS and 4FS+ b -quark total cross sections are the same to within 1%. At the LHC, however, the additional b -quark contributions to the 4FS cross section are at the +1% level and so do not completely compensate the “missing” $b\bar{b} \rightarrow Z$ contributions to the 5FS cross section. To be precise,

$$B \cdot \sigma_{\text{NNLO}}^Z(5\text{FS}, b) = 48.4 \text{ (14.5) pb} > \Delta_b \sigma^Z = 23.1 \text{ (6.6) pb} \quad (8)$$

at $\sqrt{s} = 14$ TeV (7 TeV), which results in the “full” 4FS total cross section being 2.3% (1.7%) smaller than the 5FS cross section. We interpret this as meaning that the DGLAP-resummed $[\alpha_S \ln(M_Z^2/m_b^2)]^n$ contributions that are absorbed into the b parton distribution are numerically important.

Our results are in broad agreement with the study of Ref. [85], in which the different calculational methods for heavy particles produced in association with b quarks, $gg \rightarrow Xb\bar{b}$ (4FS) versus $b\bar{b} \rightarrow X$ (5FS), were studied in detail for $X = H, Z$. In particular, it was shown

¹⁰This excludes small $\mathcal{O}(\alpha_S^2)$ contributions initiated by light quarks and gluons, e.g. $q\bar{q}, gg \rightarrow Zb\bar{b}$, in which the Z couples to b quarks.

Tevatron, $\sqrt{s} = 1.96$ TeV	$B \cdot \sigma_{\text{NNLO}}^Z(4\text{FS})$ (nb)	$B \cdot \sigma_{\text{NNLO}}^Z(5\text{FS})$ (nb)	$B \cdot \sigma_{\text{NNLO}}^Z(5\text{FS}, b)$ (nb)
σ_0^Z	0.2013	0.2016	0.0012
σ_1^Z	0.0409	0.0431	-0.0002
σ_2^Z	0.0063	0.0060	-0.0003
total	0.2485	0.2507	0.0008
$\Delta_b \sigma^Z$	0.0006	–	
total + $\Delta_b \sigma^Z$	0.2491	0.2507	

LHC, $\sqrt{s} = 7$ TeV	$B \cdot \sigma_{\text{NNLO}}^Z(4\text{FS})$ (nb)	$B \cdot \sigma_{\text{NNLO}}^Z(5\text{FS})$ (nb)	$B \cdot \sigma_{\text{NNLO}}^Z(5\text{FS}, b)$ (nb)
σ_0^Z	0.8083	0.8266	0.0202
σ_1^Z	0.1239	0.1322	-0.0020
σ_2^Z	0.0037	-0.0002	-0.0037
total	0.9359	0.9586	0.0145
$\Delta_b \sigma^Z$	0.0066	–	
total + $\Delta_b \sigma^Z$	0.9426	0.9586	

LHC, $\sqrt{s} = 14$ TeV	$B \cdot \sigma_{\text{NNLO}}^Z(4\text{FS})$ (nb)	$B \cdot \sigma_{\text{NNLO}}^Z(5\text{FS})$ (nb)	$B \cdot \sigma_{\text{NNLO}}^Z(5\text{FS}, b)$ (nb)
σ_0^Z	1.7472	1.8110	0.0641
σ_1^Z	0.2384	0.2557	-0.0050
σ_2^Z	-0.0047	-0.0153	-0.0107
total	1.9809	2.0514	0.0484
$\Delta_b \sigma^Z$	0.0231	–	
total + $\Delta_b \sigma^Z$	2.0040	2.0514	

Table 9: NNLO predictions for the total Z cross section (multiplied by leptonic branching ratio B) at the Tevatron and LHC using MSTW 2008 NNLO PDFs [1] as input, broken down into the α_S^n ($n = 0, 1, 2$) contributions, with $\{q = u, d, s, c; \alpha_S^{(4)}; 4\text{-flavour MSTW 2008 NNLO PDFs}\}$ in the 4FS calculation and $\{q = u, d, s, c, b; \alpha_S^{(5)}; 5\text{-flavour MSTW 2008 NNLO PDFs}\}$ in the 5FS calculation. The final column gives the contribution to the 5FS cross sections from processes where the Z couples directly to b quarks. The additional $\mathcal{O}(\alpha_S^2)$ contributions to the cross section arising from real and virtual b -quark processes, taken from Table 8, are added to the 4FS cross section in the last line of each sub-table.

that with the canonical choice of scale $\mu = M_Z$, the LO $gg \rightarrow Zb\bar{b}$ cross section at the LHC was a factor of two smaller than the NNLO $b\bar{b} \rightarrow Z$ cross section, consistent with our results in Eq. (8) above. It was also shown in Ref. [85] that the agreement between the 4FS and 5FS calculations improves if the scale μ is reduced to around $M_Z/3$ (found by choosing $\mu \sim \sqrt{-t}$ near the end of the collinear plateau in the quantity $-t d\sigma/dt$ for the process $gb \rightarrow Zb$). The NNLO $b\bar{b} \rightarrow Z$ cross section is approximately scale independent, while the LO $gg \rightarrow Zb\bar{b}$ cross section increases with decreasing scale, primarily because of the overall α_S^2 factor.

Of course the explicit $gg \rightarrow Zb\bar{b}$ contribution corresponds only to the $n = 1$ term in the resummed $[\alpha_S \ln(M_Z^2/m_b^2)]^n$ perturbation series implicit in the $b\bar{b} \rightarrow Z$ 5FS calculation. Complete agreement between the two schemes *would* be obtained in a fully all-orders perturbative calculation. Note that since at all collider energies $\Delta_b \sigma^Z$ is dominated by the contributions involving the $Zb\bar{b}$ final state, we would expect that higher-order corrections to the $Zb\bar{b}$ production process, which is here calculated only at leading order, will generate the $[\alpha_S \ln(M_Z^2/m_b^2)]^n$ terms implicit in the b -quark PDF. The NLO (i.e. $\mathcal{O}(\alpha_S^3)$) corrections to the $Zb\bar{b}$ total cross sections with $m_b \neq 0$ have recently been calculated [86–89]. Although the results presented in Ref. [89] impose a minimum p_T^b (> 5 GeV), the K -factor¹¹ is evidently rather independent of p_T^b at small p_T^b , suggesting that the NLO/LO K -factor for the fully inclusive $Zb\bar{b}$ cross section is approximately 1.5 for the LHC at $\sqrt{s} = 14$ TeV. It is therefore plausible that even higher-order perturbative corrections can account for the factor of 2 difference in the 4FS and 5FS cross sections, Eq. (8). This conclusion is supported by the fact that the scale dependence of the 4FS calculation for $Zb\bar{b}$ production at NLO is only mildly weaker than at LO [86–89].

In Ref. [91] it was shown that for x in the region of 0.01–0.05, the relevant region for $Z + b\bar{b}$ production at the 14 TeV LHC, the ratio of the GM-VFNS structure function F_2^b to the FFNS structure function was ~ 1.5 at LO at high scales. This represents the effect of either resumming the $[\alpha_S \ln(Q^2/m_h^2)]^n$ contributions, or keeping only the contribution of fixed order in α_S for one parton. For hadron–hadron processes we would expect the difference to be about $1.5^2 > 2$, exactly as observed. At NLO for structure functions at this x the ratio is reduced to ~ 1.1 , so inclusion of the extra $\ln(Q^2/m_h^2)$ removes much of the discrepancy present at LO. However, for hadron–hadron processes, NLO in the fixed flavour scheme only contains the extra large logarithm for one of the two incoming partons, so the ratio between the 5FS and 4FS would be roughly $1.5 \times 1.1 \approx 1.6$, again as we expect to see in practice. It would only be at NNLO in the 4FS, when the double logarithm for both incoming PDFs is included, that we would expect to see the reduction to roughly $1.1^2 \approx 1.2$ in the ratio of the 5FS to 4FS cross sections. This is a general feature, i.e. the 4FS (or 3FS) will converge to the resummed 5FS results more slowly for hadronic processes than for those in DIS.

In summary, the 5FS PDFs are clearly the most appropriate to use for inclusive quantities such as σ^Z (or σ^{dijet} , etc.) at high Q^2 scales, where resummation of the $[\alpha_S \ln(Q^2/m_b^2)]^n$ contributions is evidently important. However, for more exclusive quantities like $\sigma^{Zb\bar{b}}$, where

¹¹The K -factor is here defined as the ratio of cross sections calculated using the dynamical scale $\mu^2 = M_Z^2 + (p_T^{b,1})^2 + (p_T^{b,2})^2$, and with the standard 5-flavour CTEQ6M/CTEQ6L1 PDFs [90] at NLO/LO.

the b quarks are measured in the final state, the 4FS parton distributions are more appropriate since the 5FS calculation gives no information on the spectator b and \bar{b} quarks which must be present in the final state for the b - and \bar{b} -initiated processes. Note that if only the *total* cross section is required, without cuts imposed on the b -quarks, then a 5FS is still better, e.g. for $Zb\bar{b}$ a 5FS calculation can be used for $b\bar{b} \rightarrow Z$ at NNLO, where the b -quarks couple directly to the Z , and so there are implicitly also two b -quarks in the final state [85]. However, if cuts must be applied to the b -quarks, as is the case in the experimental measurement, then a 4FS calculation is more appropriate. Similar remarks apply to the calculation of $Hb\bar{b}$ production [92–94] and other processes where b -quarks are detected in the final state. In a recent study [95], the production of a charged Higgs boson in association with a t quark was considered in both the 4FS ($gg \rightarrow t\bar{b}H^-$ etc.) and 5FS ($gb \rightarrow tH^-$ etc.) to NLO in pQCD, using the appropriate MRST 2004 PDF sets [9,10]. The central predictions in the 5FS were shown to be approximately 40% larger than those in the 4FS. Even taking the scale uncertainty into account the 4FS and 5FS NLO cross sections are barely consistent.

An ideal calculation would combine the best features of the 4FS and 5FS so as to resum $[\alpha_S \ln(Q^2/m_b^2)]^n$ terms while also retaining a finite m_b dependence in the partonic cross section (rather than setting m_b to zero as done in the 5FS). This matching has, of course, been done for structure functions in DIS using different variants of the GM-VFNS, but applications to hadron collider cross sections are more involved and have so far been limited (see Ref. [96] for an application of the GM-VFNS to the p_T spectrum in heavy-flavour hadroproduction). However, for processes where the hard scale is, for example, $Q^2 \sim M_Z^2$, then the GM-VFNS calculation will differ from the ZM-VFNS (5FS) only by terms $\mathcal{O}(m_b^2/M_Z^2 \sim 0.3\%)$. We would therefore expect the complete GM-VFNS calculation to give results very close to the pure ZM-VFNS (5FS) for the total cross section.

Note that rather than producing separate 4-flavour PDFs for use in a 4FS calculation, an alternative approach (e.g. used at NLO in Refs. [97,98]) is to use the conventional 5-flavour PDFs, then pass to the 4-flavour scheme using counterterms given in Ref. [96]. However, these counterterms [96] are equivalent to using the inverse of transition matrix elements, but only out to order α_S . One could indeed use the transition matrix elements themselves to go from 4-flavour to 5-flavour PDFs, except this would not sum the logarithmic terms, $[\alpha_S \ln(Q^2/m_b^2)]^n$, in the PDF evolution.¹² Hence, the use of counterterms [96] is a less complete way of going from a 5FS to a 4FS, and instead, we recommend that dedicated 4-flavour PDFs be used in 4FS calculations.¹³ Previously, a major advantage of using 5-flavour PDFs with counterterms was that eigenvector PDF sets to calculate PDF uncertainties were not made available for existing

¹²See Fig. 9 of Ref. [80] for a comparison of 5-flavour NNLO PDFs obtained from 3-flavour PDFs either by evolution or by applying fixed-order matching conditions; the differences will be larger at NLO.

¹³However, for the 4FS calculation of t -channel single-top production at the Tevatron and LHC [97], it was explicitly checked that results obtained with the dedicated 4-flavour MRST set [9] were consistent (within the numerical integration precision) with those obtained with the corresponding 5-flavour MRST set [10] plus appropriate counterterms [96]. We thank R. Frederix and F. Tramontano for discussions on this issue.

4-flavour PDFs [9]. However, we have now provided eigenvector PDF sets also for the 4-flavour PDFs, therefore this advantage no longer holds.

5 Conclusions

We have repeated the NLO and NNLO MSTW 2008 global PDF analyses [1] for a range of heavy-quark masses about their “default” values $m_c = 1.40$ GeV and $m_b = 4.75$ GeV. For the charm quark, we found that the global data prefer the values $m_c = 1.45$ (1.26) GeV at NLO (NNLO). The most discriminating data are, as anticipated, the HERA data for F_2^c [44–50]. On the other hand, for the bottom quark, the data included in the global fit (excluding F_2^b) do not put a meaningful constraint on the value of m_b , while the HERA F_2^b data slightly favour $m_b \approx 4.75$ –5 GeV. We pointed out that precise determinations of the heavy-quark masses in the $\overline{\text{MS}}$ scheme are affected by poorly convergent perturbative series in the conversion to the pole masses, particularly for the case of the charm quark. Recent precise combined HERA data on σ_r^{NC} [79] and F_2^c [74] will in future be able to narrow the favoured range of the charm-quark pole mass m_c . Note, however, that uncertainties from the choice of GM-VFNS [64] mean that the favoured value of m_c will be correlated to some extent with the particular choice of GM-VFNS, although this correlation will be much smaller at NNLO than at NLO, as will other uncertainties arising from the choice of GM-VFNS [64].

We explored the effect of the values of the heavy-quark masses on W , Z and Higgs production at the Tevatron and LHC. Varying the charm mass by ± 0.15 GeV changes the cross sections by $\pm 1\%$ or less at Tevatron energies and by $\pm 2\%$ at the LHC energy of $\sqrt{s} = 14$ TeV. The various weak boson cross-section *ratios* are essentially unchanged. The predictions for W , Z and Higgs cross sections are much less dependent on the value taken for m_b . We provided a recommendation on how to include the uncertainty arising from the choices of m_c and m_b in a generic cross-section calculation.

We also presented PDF sets obtained in a framework with different active numbers of quark flavours, as done previously in the context of the MRST 2004 analysis [9]. Explicitly, we determined 4-flavour PDF sets in which charm becomes an active parton, but bottom does not, and 3-flavour PDF sets where charm and bottom are not partons, but only appear in the final state. The analogous 5-flavour parton sets are simply those of MSTW 2008 [1]. Of course, the latter, which in the absence of top corresponds to PDFs of a (general-mass) variable flavour number scheme, are generally to be preferred, particularly for inclusive quantities at high Q^2 scales where the resummation of the $[\alpha_S \ln(Q^2/m_b^2)]^n$ contributions is essential. However, for more exclusive processes, such as $Zb\bar{b}$, $Hb\bar{b}$, \dots , where b -quarks are observed in the final state, the 4-flavour parton distributions are more appropriate. For illustration, we computed the various components of the Z production cross section to $\mathcal{O}(\alpha_S^2)$ at the Tevatron and LHC, and compared the predictions obtained using the 4FS and 5FS (\equiv MSTW 2008 [1]) parton sets.

The additional grids for all PDF sets discussed in this paper are made publicly available [60], for use either with the standalone MSTW interpolation code or via the LHAPDF interface [99]. To be precise, grids for the following PDF sets are made available:

- For the default quark masses, $m_c = 1.40$ GeV and $m_b = 4.75$ GeV, we provide LO, NLO and NNLO grids for 3- and 4-flavour PDFs (central set and 40 eigenvector sets at both 68% and 90% C.L.). These grids complement the existing grids for the 5-flavour PDFs.
- For m_c in the range 1.05 GeV to 1.75 GeV (in steps of 0.05 GeV), we provide NLO and NNLO grids for 3- and 5-flavour PDFs (central set only) for both free and fixed $\alpha_S(M_Z^2)$.
- For m_b in the range 4.00 GeV to 5.50 GeV (in steps of 0.25 GeV), we provide NLO and NNLO grids for 4- and 5-flavour PDFs (central set only) for free $\alpha_S(M_Z^2)$ only.

These additional grids should prove to be useful in future for detailed studies of a variety of collider processes involving heavy quarks.

A Appendix

We consider the b -quark contributions to the 4FS calculation, closely following the discussion in Ref. [83]. First, we have the two-loop corrections to the $q + \bar{q} \rightarrow Z$ Born process, examples of which are shown in Fig. 11(a) and (b). In the notation of Ref. [83],

$$W_{q\bar{q}}^Z = \delta(1 - \hat{\tau}) C_F T_f \left(\frac{\alpha_S}{\pi} \right)^2 \left[2a_q a_Q G_1(\rho_b) + \frac{1}{2} (v_q^2 + a_q^2) F(\rho_b) \right], \quad (\text{A.1})$$

with $\rho_b = m_b^2/M_Z^2 \approx 2.7 \times 10^{-3}$. The functions F and G_1 are defined in Refs. [83] and [84] respectively. Since in practice $\rho_b \ll 1$, we can use the following small-mass expansions:

$$F(\rho) \simeq -\frac{4}{9}L^3 + \frac{38}{9}L^2 + \left(\frac{16}{3}\zeta_2 - \frac{530}{27} \right) L + \frac{3355}{81} - \frac{152}{9}\zeta_2 - \frac{16}{3}\zeta_3 \\ + \rho \left(16L^2 - 32L + 128 - \frac{192}{3}\zeta_2 \right) + \mathcal{O}(\rho^2), \quad (\text{A.2})$$

$$G_1(\rho) \simeq 4\rho(-2\zeta_2 L + 2\zeta_3 - 3) + \mathcal{O}(\rho^2), \quad (\text{A.3})$$

with $L = \ln(1/\rho) \approx 5.9$ for $\rho = \rho_b$. The contributions to the total Z cross section from these loop diagrams are given in the first row of Table 8. They are numerically very small and negative (positive) at the LHC (Tevatron).¹⁴

¹⁴Even though the function $G_1(\rho)$ is suppressed by a power of ρ relative to $F(\rho)$ at small ρ , it gives a comparable contribution to the cross section. This is because F has a zero close to the physical value $\rho = \rho_b$.

Next we have the one-loop corrections to the $2 \rightarrow 2$ processes $q + \bar{q} \rightarrow Z + g$ and $g + q(\bar{q}) \rightarrow Z + q(\bar{q})$, examples of which are shown in Fig. 11(c) and (d):

$$W_{q\bar{q}}^Z = \frac{1}{2} a_q a_Q C_F T_f \left(\frac{\alpha_S}{\pi} \right)^2 \left[\frac{1 + \hat{\tau}}{1 - \hat{\tau}} \{-2 + 2\hat{\tau} (J_1(4\rho_b \hat{\tau}) - J_1(4\rho_b))\} - 4\rho_b \hat{\tau} (J_2(4\rho_b \hat{\tau}) - J_2(4\rho_b)) \right], \quad (\text{A.4})$$

$$W_{gg}^Z = \frac{1}{2} a_q a_Q T_f^2 \left(\frac{\alpha_S}{\pi} \right)^2 H_1(\hat{\tau}, \rho_b), \quad (\text{A.5})$$

where $\hat{s} = \hat{\tau}^{-1} M_Z^2$ and the functions H_1 , J_1 and J_2 are defined in Ref. [84]. The following small-mass approximations are again useful:

$$\begin{aligned} H_1(\tau, 0) &= 2\tau \left[\left\{ 2(\tau - 1) + \ln \left(\frac{1}{\tau} \right) \right\} \ln \left(\frac{1 - \tau}{\tau} \right) + \text{Li}_2 \left(\frac{\tau - 1}{\tau} \right) \right] + 2(1 - \tau), \\ J_1(\rho) &\simeq L + \ln 4 - 2 - \frac{\rho}{2} (L + \ln 4 + 1) + \mathcal{O}(\rho^2), \\ J_2(\rho) &\simeq \frac{1}{2} ((L + \ln 4)^2 - \pi^2) - \frac{\rho}{2} (L + \ln 4) + \mathcal{O}(\rho^2). \end{aligned} \quad (\text{A.6})$$

Finally, we have the $2 \rightarrow 3$ processes

$$q + \bar{q} \rightarrow Z + b + \bar{b}, \quad g + g \rightarrow Z + b + \bar{b}, \quad (\text{A.7})$$

see Fig. 11(e) and (f). The calculation of these is in principle straightforward, with matrix elements squared integrated over three-body phase space. The non-zero b -quark mass makes these contributions infra-red and collinear finite, i.e. the singularities present for massless quarks are replaced by terms with logarithmic ($\ln(M_Z^2/m_b^2)$) behaviour in the small m_b limit. We use the MCFM implementation [100] of the matrix elements and phase space, with exactly the same parameter choice as in the previous MSTW calculations. The results are given in Table 8. Note that the gg contribution is larger than the $q\bar{q}$ contribution at the LHC, while the converse is true at the Tevatron.

References

- [1] A. D. Martin, W. J. Stirling, R. S. Thorne and G. Watt, Eur. Phys. J. C **63** (2009) 189 [arXiv:0901.0002 [hep-ph]].
- [2] A. D. Martin, W. J. Stirling, R. S. Thorne and G. Watt, Phys. Lett. B **652** (2007) 292 [arXiv:0706.0459 [hep-ph]].
- [3] H. L. Lai, M. Guzzi, J. Huston, Z. Li, P. M. Nadolsky, J. Pumplin and C. P. Yuan, Phys. Rev. D **82** (2010) 074024 [arXiv:1007.2241 [hep-ph]].
- [4] P. M. Nadolsky *et al.*, Phys. Rev. D **78** (2008) 013004 [arXiv:0802.0007 [hep-ph]].

- [5] R. D. Ball, L. Del Debbio, S. Forte, A. Guffanti, J. I. Latorre, J. Rojo and M. Ubiali, Nucl. Phys. B **838** (2010) 136 [arXiv:1002.4407 [hep-ph]].
- [6] A. D. Martin, W. J. Stirling, R. S. Thorne and G. Watt, Eur. Phys. J. C **64** (2009) 653 [arXiv:0905.3531 [hep-ph]].
- [7] H. L. Lai, J. Huston, Z. Li, P. Nadolsky, J. Pumplin, D. Stump and C. P. Yuan, Phys. Rev. D **82** (2010) 054021 [arXiv:1004.4624 [hep-ph]].
- [8] F. Demartin, S. Forte, E. Mariani, J. Rojo and A. Vicini, Phys. Rev. D **82** (2010) 014002 [arXiv:1004.0962 [hep-ph]].
- [9] A. D. Martin, W. J. Stirling and R. S. Thorne, Phys. Lett. B **636** (2006) 259 [arXiv:hep-ph/0603143].
- [10] A. D. Martin, R. G. Roberts, W. J. Stirling and R. S. Thorne, Phys. Lett. B **604** (2004) 61 [arXiv:hep-ph/0410230].
- [11] M. Buza, Y. Matiounine, J. Smith and W. L. van Neerven, Eur. Phys. J. C **1** (1998) 301 [arXiv:hep-ph/9612398].
- [12] I. Bierenbaum, J. Blumlein and S. Klein, Nucl. Phys. B **820** (2009) 417 [arXiv:0904.3563 [hep-ph]].
- [13] E. Laenen, S. Riemersma, J. Smith and W. L. van Neerven, Nucl. Phys. B **392**, 162 (1993).
- [14] R. S. Thorne, Phys. Rev. D **73** (2006) 054019 [arXiv:hep-ph/0601245].
- [15] S. Catani, M. Ciafaloni and F. Hautmann, Nucl. Phys. B **366** (1991) 135.
- [16] E. Laenen and S. O. Moch, Phys. Rev. D **59** (1999) 034027 [arXiv:hep-ph/9809550].
- [17] S. Alekhin and S. Moch, Phys. Lett. B **672** (2009) 166 [arXiv:0811.1412 [hep-ph]].
- [18] N. A. L. Presti, H. Kawamura, S. Moch and A. Vogt, PoS **DIS2010** (2010) 163 [arXiv:1008.0951 [hep-ph]].
- [19] B. W. Harris and J. Smith, Nucl. Phys. B **452** (1995) 109 [arXiv:hep-ph/9503484];
- [20] B. W. Harris and J. Smith, Phys. Rev. D **57** (1998) 2806 [arXiv:hep-ph/9706334].
- [21] S. Frixione, P. Nason and B. R. Webber, JHEP **0308** (2003) 007 [arXiv:hep-ph/0305252].
- [22] A. C. Benvenuti *et al.* [BCDMS Collaboration], Phys. Lett. B **223** (1989) 485.
- [23] A. C. Benvenuti *et al.* [BCDMS Collaboration], Phys. Lett. B **237** (1990) 592.

- [24] M. Arneodo *et al.* [New Muon Collaboration], Nucl. Phys. B **483** (1997) 3 [arXiv:hep-ph/9610231].
- [25] M. Arneodo *et al.* [New Muon Collaboration], Nucl. Phys. B **487** (1997) 3 [arXiv:hep-ex/9611022].
- [26] M. R. Adams *et al.* [E665 Collaboration], Phys. Rev. D **54** (1996) 3006.
- [27] L. W. Whitlow, E. M. Riordan, S. Dasu, S. Rock and A. Bodek, Phys. Lett. B **282** (1992) 475.
- [28] L. W. Whitlow, Ph.D. thesis, Stanford University, 1990, SLAC-0357.
- [29] L. W. Whitlow, S. Rock, A. Bodek, E. M. Riordan and S. Dasu, Phys. Lett. B **250** (1990) 193.
- [30] J. C. Webb, Ph.D. thesis, New Mexico State University, 2002, arXiv:hep-ex/0301031; Paul E. Reimer, private communication (for the radiative corrections).
- [31] R. S. Towell *et al.* [FNAL E866/NuSea Collaboration], Phys. Rev. D **64** (2001) 052002 [arXiv:hep-ex/0103030].
- [32] M. Goncharov *et al.* [NuTeV Collaboration], Phys. Rev. D **64** (2001) 112006 [arXiv:hep-ex/0102049].
- [33] M. Tzanov *et al.* [NuTeV Collaboration], Phys. Rev. D **74** (2006) 012008 [arXiv:hep-ex/0509010].
- [34] G. Onengut *et al.* [CHORUS Collaboration], Phys. Lett. B **632** (2006) 65.
- [35] E. M. Lobodzinska [H1 Collaboration], arXiv:hep-ph/0311180.
- [36] C. Adloff *et al.* [H1 Collaboration], Eur. Phys. J. C **21** (2001) 33 [arXiv:hep-ex/0012053].
- [37] C. Adloff *et al.* [H1 Collaboration], Eur. Phys. J. C **19** (2001) 269 [arXiv:hep-ex/0012052].
- [38] C. Adloff *et al.* [H1 Collaboration], Eur. Phys. J. C **30** (2003) 1 [arXiv:hep-ex/0304003].
- [39] J. Breitweg *et al.* [ZEUS Collaboration], Eur. Phys. J. C **7** (1999) 609 [arXiv:hep-ex/9809005].
- [40] S. Chekanov *et al.* [ZEUS Collaboration], Eur. Phys. J. C **21** (2001) 443 [arXiv:hep-ex/0105090].
- [41] S. Chekanov *et al.* [ZEUS Collaboration], Eur. Phys. J. C **28** (2003) 175 [arXiv:hep-ex/0208040].

- [42] S. Chekanov *et al.* [ZEUS Collaboration], Phys. Rev. D **70** (2004) 052001 [arXiv:hep-ex/0401003].
- [43] S. Chekanov *et al.* [ZEUS Collaboration], Eur. Phys. J. C **32** (2003) 1 [arXiv:hep-ex/0307043].
- [44] C. Adloff *et al.* [H1 Collaboration], Z. Phys. C **72** (1996) 593 [arXiv:hep-ex/9607012].
- [45] C. Adloff *et al.* [H1 Collaboration], Phys. Lett. B **528** (2002) 199 [arXiv:hep-ex/0108039].
- [46] A. Aktas *et al.* [H1 Collaboration], Eur. Phys. J. C **45** (2006) 23 [arXiv:hep-ex/0507081].
- [47] A. Aktas *et al.* [H1 Collaboration], Eur. Phys. J. C **40** (2005) 349 [arXiv:hep-ex/0411046].
- [48] J. Breitweg *et al.* [ZEUS Collaboration], Eur. Phys. J. C **12** (2000) 35 [arXiv:hep-ex/9908012].
- [49] S. Chekanov *et al.* [ZEUS Collaboration], Phys. Rev. D **69** (2004) 012004 [arXiv:hep-ex/0308068].
- [50] S. Chekanov *et al.* [ZEUS Collaboration], JHEP **0707** (2007) 074 [arXiv:0704.3562 [hep-ex]].
- [51] A. Aktas *et al.* [H1 Collaboration], Phys. Lett. B **653** (2007) 134 [arXiv:0706.3722 [hep-ex]].
- [52] S. Chekanov *et al.* [ZEUS Collaboration], Phys. Lett. B **547** (2002) 164 [arXiv:hep-ex/0208037].
- [53] S. Chekanov *et al.* [ZEUS Collaboration], Nucl. Phys. B **765** (2007) 1 [arXiv:hep-ex/0608048].
- [54] V. M. Abazov *et al.* [DØ Collaboration], Phys. Rev. Lett. **101** (2008) 062001 [arXiv:0802.2400 [hep-ex]].
- [55] A. Abulencia *et al.* [CDF - Run II Collaboration], Phys. Rev. D **75** (2007) 092006 [Erratum-ibid. D **75** (2007) 119901] [arXiv:hep-ex/0701051].
- [56] V. M. Abazov *et al.* [DØ Collaboration], Phys. Rev. D **77** (2008) 011106 [arXiv:0709.4254 [hep-ex]].
- [57] D. Acosta *et al.* [CDF Collaboration], Phys. Rev. D **71** (2005) 051104 [arXiv:hep-ex/0501023].
- [58] V. M. Abazov *et al.* [DØ Collaboration], Phys. Rev. D **76** (2007) 012003 [arXiv:hep-ex/0702025].

- [59] J. Han *et al.* [CDF Collaboration], “ $d\sigma/dy$ distribution of Drell–Yan dielectron pairs”, Public Note, May 2008, <http://www-cdf.fnal.gov/physics/ewk/2008/dszdy/>.
- [60] <http://projects.hepforge.org/mstwpdf/>
- [61] F. D. Aaron *et al.* [H1 Collaboration], Eur. Phys. J. C **65** (2010) 89 [arXiv:0907.2643 [hep-ex]].
- [62] H. Abramowicz *et al.* [ZEUS collaboration], Eur. Phys. J. C **69** (2010) 347 [arXiv:1005.3396 [hep-ex]].
- [63] S. Chekanov *et al.* [ZEUS Collaboration], Eur. Phys. J. C **65** (2010) 65 [arXiv:0904.3487 [hep-ex]].
- [64] R. S. Thorne, PoS **DIS2010** (2010) 053 [arXiv:1006.5925 [hep-ph]].
- [65] C. Amsler *et al.* [Particle Data Group], Phys. Lett. B **667** (2008) 1.
- [66] K. G. Chetyrkin, J. H. Kuhn, A. Maier, P. Maierhofer, P. Marquard, M. Steinhauser and C. Sturm, Phys. Rev. D **80** (2009) 074010 [arXiv:0907.2110 [hep-ph]].
- [67] S. Narison, Phys. Lett. B **693** (2010) 559 [arXiv:1004.5333 [hep-ph]].
- [68] K. G. Chetyrkin and M. Steinhauser, Nucl. Phys. B **573** (2000) 617 [arXiv:hep-ph/9911434].
- [69] K. Melnikov and T. v. Ritbergen, Phys. Lett. B **482** (2000) 99 [arXiv:hep-ph/9912391].
- [70] J. H. Kuhn, Nucl. Phys. Proc. Suppl. **181-182** (2008) 141.
- [71] I. I. Y. Bigi, M. A. Shifman, N. G. Uraltsev and A. I. Vainshtein, Phys. Rev. D **50** (1994) 2234 [arXiv:hep-ph/9402360].
- [72] M. Beneke and V. M. Braun, Nucl. Phys. B **426** (1994) 301 [arXiv:hep-ph/9402364].
- [73] A. H. Hoang and A. V. Manohar, Phys. Lett. B **633** (2006) 526 [arXiv:hep-ph/0509195].
- [74] HERA Heavy Flavour Combination Group, “Combination of $F_2^{c\bar{c}}$ from DIS measurements at HERA”, H1prelim-09-171, ZEUS-prel-09-015.
- [75] J. J. Aubert *et al.* [European Muon Collaboration], Nucl. Phys. B **213** (1983) 31.
- [76] A. M. Cooper-Sarkar, PoS **DIS2010** (2010) 023 [arXiv:1006.4471 [hep-ph]].
- [77] M. Gluck, P. Jimenez-Delgado and E. Reya, Eur. Phys. J. C **53** (2008) 355 [arXiv:0709.0614 [hep-ph]];
- [78] P. Jimenez-Delgado and E. Reya, Phys. Rev. D **79** (2009) 074023 [arXiv:0810.4274 [hep-ph]].

- [79] F. D. Aaron *et al.* [H1 and ZEUS Collaborations], JHEP **1001** (2010) 109 [arXiv:0911.0884 [hep-ex]].
- [80] S. Alekhin, J. Blumlein, S. Klein and S. Moch, Phys. Rev. D **81** (2010) 014032 [arXiv:0908.2766 [hep-ph]].
- [81] R. S. Thorne and W. K. Tung, arXiv:0809.0714 [hep-ph].
- [82] M. Buza and W. L. van Neerven, Nucl. Phys. B **500** (1997) 301 [arXiv:hep-ph/9702242].
- [83] P. J. Rijken and W. L. van Neerven, Phys. Rev. D **52**, 149 (1995) [arXiv:hep-ph/9501373].
- [84] R. J. Gonsalves, C. M. Hung and J. Pawlowski, Phys. Rev. D **46** (1992) 4930.
- [85] F. Maltoni, T. McElmurry and S. Willenbrock, Phys. Rev. D **72** (2005) 074024 [arXiv:hep-ph/0505014].
- [86] F. Febres Cordero, L. Reina and D. Wackerroth, Phys. Rev. D **74** (2006) 034007 [arXiv:hep-ph/0606102];
- [87] F. Febres Cordero, L. Reina and D. Wackerroth, Phys. Rev. D **78** (2008) 074014 [arXiv:0806.0808 [hep-ph]];
- [88] F. Febres Cordero, L. Reina and D. Wackerroth, Phys. Rev. D **80** (2009) 034015 [arXiv:0906.1923 [hep-ph]].
- [89] F. Febres Cordero and L. Reina, “ $Zb\bar{b}$ for CMS, Study I”, private communication.
- [90] J. Pumplin, D. R. Stump, J. Huston, H. L. Lai, P. M. Nadolsky and W. K. Tung, JHEP **0207** (2002) 012 [arXiv:hep-ph/0201195].
- [91] R. S. Thorne and R. G. Roberts, Phys. Rev. D **57** (1998) 6871 [arXiv:hep-ph/9709442].
- [92] S. Dittmaier, M. Kramer and M. Spira, Phys. Rev. D **70** (2004) 074010 [arXiv:hep-ph/0309204].
- [93] S. Dawson, C. B. Jackson, L. Reina and D. Wackerroth, Phys. Rev. D **69** (2004) 074027 [arXiv:hep-ph/0311067].
- [94] J. M. Campbell *et al.*, arXiv:hep-ph/0405302.
- [95] S. Dittmaier, M. Kramer, M. Spira and M. Walser, arXiv:0906.2648 [hep-ph].
- [96] M. Cacciari, M. Greco and P. Nason, JHEP **9805** (1998) 007 [arXiv:hep-ph/9803400].
- [97] J. M. Campbell, R. Frederix, F. Maltoni and F. Tramontano, Phys. Rev. Lett. **102** (2009) 182003 [arXiv:0903.0005 [hep-ph]].

- [98] J. M. Campbell, R. Frederix, F. Maltoni and F. Tramontano, JHEP **0910** (2009) 042 [arXiv:0907.3933 [hep-ph]].
- [99] M. R. Whalley, D. Bourilkov and R. C. Group, arXiv:hep-ph/0508110; LHAPDF code from <http://projects.hepforge.org/lhapdf/>.
- [100] J. M. Campbell and R. K. Ellis, Phys. Rev. D **62** (2000) 114012 [arXiv:hep-ph/0006304]; MCFM code from <http://mcfm.fnal.gov/>.